Application of an inverse method to interpret $^{231}Pa/^{230}Th$ observations from marine sediments

Andrea Burke,[1] Olivier Marchal,[2] Louisa I. Bradtmiller,[3] Jerry F. McManus,[4] and Roger François[5]

Received 28 June 2010; revised 10 December 2010; accepted 28 December 2010; published 16 March 2011.

[1] Records of $^{231}Pa/^{230}Th$ from Atlantic sediments have been interpreted to reflect changes in ocean circulation during the geologic past. Such interpretations should be tested with due regard to the limited spatial coverage of $^{231}Pa/^{230}Th$ data and the uncertainties in our current understanding of the behavior of both nuclides in the ocean. Here an inverse method is used to evaluate the information contained in $^{231}Pa/^{230}Th$ compilations for the Holocene, Last Glacial Maximum (LGM), and Heinrich Event 1 (H1). An estimate of the abyssal circulation in the modern Atlantic Ocean is obtained by combining hydrographic observations and dynamical constraints. Then sediment $^{231}Pa/^{230}Th$ data for each time interval are combined with an advection-scavenging model in order to determine their (in)consistency with the modern circulation estimate. We find that the majority of sediment $^{231}Pa/^{230}Th$ data for the Holocene, LGM, or H1 can be brought into consistency with the modern circulation if plausible assumptions are made about the large-scale distribution of ^{231}Pa and about model uncertainties. Moreover, the adjustments in the data needed to reach compatibility with a hypothetical state of no flow (no advection) are positively biased for each time interval, suggesting that the $^{231}Pa/^{230}Th$ data (including that for H1) are more consistent with a persistence of some circulation than with no circulation. Our study does not imply that earlier claims of a circulation change during the LGM or H1 are inaccurate, but that these claims cannot be given a rigorous basis given the current uncertainties involved in the analysis of the $^{231}Pa/^{230}Th$ data.

Citation: Burke, A., O. Marchal, L. I. Bradtmiller, J. F. McManus, and R. François (2011), Application of an inverse method to interpret $^{231}Pa/^{230}Th$ observations from marine sediments, *Paleoceanography*, *26*, PA1212, doi:10.1029/2010PA002022.

1. Introduction

[2] One of the major goals of paleoceanography is to understand past changes in ocean circulation. This is important because the ocean is a major transporter of heat, accounting at maximum for about half of the meridional heat flux of the combined atmosphere-ocean system in the tropics [e.g., *Trenberth and Caron*, 2001; *Wunsch*, 2005; *Fasullo and Trenberth*, 2008]. As a result, changes in ocean circulation can potentially affect climate locally, regionally and/or globally.

[3] Recently, downcore records of the ratio of two radioisotopes in sediment, protactinium-231 and thorium-230, have been used to infer past changes in the strength or structure of the meridional overturning circulation (MOC) in the Atlantic Ocean [e.g., *Yu et al.*, 1996; *McManus et al.*, 2004; *Gherardi et al.*, 2005; *Hall et al.*, 2006; *Gherardi et al.*, 2009; *Guihou et al.*, 2010; *Negre et al.*, 2010]. ^{231}Pa and ^{230}Th are produced in seawater in a nearly constant ratio (0.093) from the radioactive decay of ^{235}U and ^{234}U, respectively [*Yu et al.*, 1996]. According to current understanding, ^{231}Pa and ^{230}Th are removed from the water column through a reversible exchange with slowly sinking particles, a process referred to as "particle scavenging" [*Nozaki et al.*, 1981; *Bacon and Anderson*, 1982]. While both isotopes are particle reactive, ^{230}Th appears in general to be more readily adsorbed onto sinking particles, resulting in a shorter residence time (estimated to ~20–40 years) than that of ^{231}Pa (~100–200 years) [*Anderson et al.*, 1983; *Henderson and Anderson*, 2003; *McManus et al.*, 2004]. The residence time of ^{231}Pa is of the same order of magnitude as the time it would take to ventilate the deep Atlantic basins via replenishment by the southward flowing North Atlantic Deep Water (NADW) [*Broecker*, 1979]. Thus, a significant fraction (~45%) of ^{231}Pa produced in the Atlantic Ocean would be exported to the Southern Ocean today [*Yu et al.*, 1996]. Such export would help explain the ^{231}Pa deficit in core top sediments from the Atlantic, whose $^{231}Pa_{xs,0}/^{230}Th_{xs,0}$ ratios average about half of the production ratio in the water column ([*Yu et al.*, 1996]; the subscript "xs,0" refers to excess ^{231}Pa or ^{230}Th that is not supported by radioactive decay of U present in the mineral

[1] MIT/WHOI Joint Program in Oceanography, Woods Hole Oceanographic Institution, Woods Hole, Massachusetts, USA.
[2] Department of Geology and Geophysics, Woods Hole Oceanographic Institution, Woods Hole, Massachusetts, USA.
[3] Department of Environmental Studies, Macalester College, St. Paul, Minnesota, USA.
[4] Department of Earth and Environmental Science, Lamont-Doherty Earth Observatory, Palisades, New York, USA.
[5] Department of Earth and Ocean Sciences, University of British Columbia, Vancouver, British Columbia, Canada.

0883-8305/11/2010PA002022

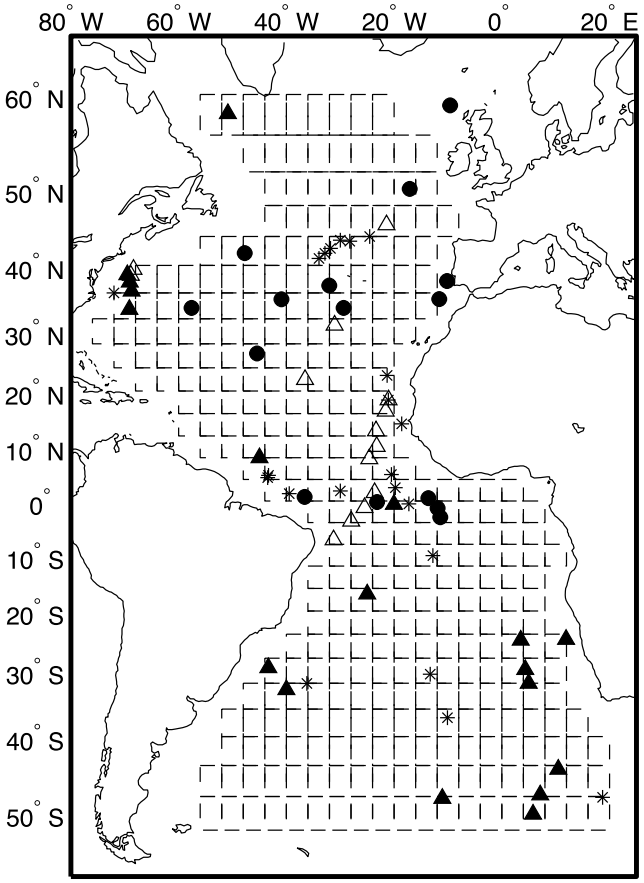

Figure 1. Geographic locations of (1) water column stations with total ^{231}Pa activity data (filled triangle) or dissolved ^{231}Pa activity data (open triangle) and (2) sediment cores with $^{231}Pa/^{230}Th$ measurements for the Holocene, LGM, and H1 (filled circle). Locations of cores with only $^{231}Pa/^{230}Th$ measurements for the Holocene and LGM are marked with an asterisk. The model grid is also outlined.

lattices of the sediment, and decay corrected for the time of deposition. Hereafter, $^{231}Pa_{xs,0}/^{230}Th_{xs,0}$ will be noted as $^{231}Pa/^{230}Th$).

[4] *Yu et al.* [1996] compiled $^{231}Pa/^{230}Th$ ratios measured in Atlantic sediments deposited during the Last Glacial Maximum (LGM) and the Holocene. They found that the average glacial and Holocene $^{231}Pa/^{230}Th$ ratios in the Atlantic Ocean north of the polar front (50°S) are not significantly different. Hence, *Yu et al.* inferred that the export of ^{231}Pa to the Southern Ocean by the MOC was similar during both periods.

[5] Circulation-scavenging models, however, have shown that the Atlantic mean $^{231}Pa/^{230}Th$ might not be a sensitive indicator of the strength of the MOC, and that the spatial distribution of the cores is important. *Marchal et al.* [2000] showed that the average $^{231}Pa/^{230}Th$ for the whole Atlantic Ocean is less sensitive to changes in the MOC than the average $^{231}Pa/^{230}Th$ for the North Atlantic. Given the uncertainties of these averages, the MOC during the LGM could have been reduced by as much as 30% compared to present. *Siddall et al.* [2007] showed that if the Atlantic MOC is slowed or shut down, ^{231}Pa is scavenged in areas with high particle flux, making those areas the most sensitive to the strength of the MOC. Therefore, unless areas of high particle flux are adequately sampled, the mean $^{231}Pa/^{230}Th$ of the North Atlantic would be biased to lower values, resulting in an overestimation of the ^{231}Pa export to the Southern Ocean via the meridional circulation.

[6] Results from a box model [*Yu et al.*, 1996] and a zonally averaged circulation model [*Marchal et al.*, 2000] have suggested that high-resolution $^{231}Pa/^{230}Th$ records from Atlantic sediments could capture variations in the strength of the MOC on centennial to millennial timescales. Thus far, $^{231}Pa/^{230}Th$ records with high resolution have been generated from sediments dating back to about 20 kyr B.P. (before present) in six different cores from the North Atlantic [*McManus et al.*, 2004; *Gherardi et al.*, 2005; *Hall et al.*, 2006; *Gherardi et al.*, 2009] (Figure 1). A notable feature in four of these cores (OCE326-GGC5, SU81-18, SU90-44, and MD95-2027) is the occurrence of high $^{231}Pa/^{230}Th$ ratios during Heinrich Event 1 (H1; between 15 and 17 kyr B.P.), nearing the production ratio of these two nuclides in the water column (0.093). Heinrich events are typically identified in North Atlantic sediment cores as layers of coarse-grained lithogenic fragments most likely transported by icebergs, otherwise known as "ice-rafted debris" [*Heinrich*, 1988; *Hemming*, 2004]. The increase in sediment $^{231}Pa/^{230}Th$ during H1 has been interpreted as a reduction in the southward export of ^{231}Pa, owing to a slow down or halting of the MOC [*McManus et al.*, 2004].

[7] However, this interpretation has not gone unchallenged. First, changes in the abundance, vertical flux, and/or chemical composition of particles scavenging Th and Pa in the water column could also contribute to downcore variations of $^{231}Pa/^{230}Th$. Elevated sedimentary $^{231}Pa/^{230}Th$ could result from a large abundance or flux of biogenic silica in the water column since biogenic silica (opal) scavenges Pa more readily than Th [e.g., *Chase et al.*, 2002]. Such influence likely occurs in the Southern Ocean [*Walter et al.*, 1997]. It has also been inferred in a core from the eastern North Atlantic, where throughout the Holocene high sedimentary $^{231}Pa/^{230}Th$ (ranging from 0.091 to 0.097) coincides with elevated diatom flux [*Hall et al.*, 2006]. Note that, in this core, $^{231}Pa/^{230}Th$ stays constant as the diatom flux increases during the Holocene and $^{231}Pa/^{230}Th$ increases as the diatom flux vanishes from 20 to 10 kyr B.P., so a role of biogenic silica in downcore variations of $^{231}Pa/^{230}Th$ remains still to be established. More recently, *Lippold et al.* [2009] measured $^{231}Pa/^{230}Th$ in a Bermuda Rise core near OCE326-GGC5 [*McManus et al.*, 2004]. They found that the high $^{231}Pa/^{230}Th$ values during H1 (and also during Heinrich Events 2 and 3) correspond with peaks in diatom abundance. Likewise, *Gil et al.* [2009] found that the high $^{231}Pa/^{230}Th$ values during H1 in OCE326-GGC5 nearly coincide with an interval of higher diatom content in a nearby core, concluding that opal productivity may have biased earlier interpretation of these values in terms of MOC.

[8] Second, a complete cessation of the Atlantic MOC during H1 is not consistent with some other sediment data.

Keigwin and Boyle [2008] reported "apparent ventilation ages" based on the difference in radiocarbon years between deep dwelling bivalves and coeval planktonic foraminifera picked from a sediment core near Bermuda. They found that the apparent ventilation age (assuming constant end-member composition) was about 1000 years during H1, in contrast to that of about 1500 years during the LGM estimated from the ^{14}C age difference between bivalves and planktonic foraminifera. These results appear inconsistent with $^{231}Pa/^{230}Th$ records from the Bermuda Rise [*McManus et al.*, 2004] if each proxy is interpreted strictly in terms of circulation: $^{231}Pa/^{230}Th$ ratios from the LGM are lower than those from H1, implying a more vigorous circulation during the LGM, whereas the apparent ventilation ages imply that the H1 circulation was more vigorous. Keigwin and Boyle explained the apparent inconsistency between the two proxy records by hypothesizing that the high $^{231}Pa/^{230}Th$ observed during H1 result from high diatom (opal) fluxes, as apparently supported by diatom abundance data reported in subsequent work [*Gil et al.*, 2009; *Lippold et al.*, 2009]. Note that the issue of data consistency may not lie solely in reevaluating $^{231}Pa/^{230}Th$ (for a critical discussion of ^{14}C see, e.g., *Wunsch* [2003]).

[9] The debate about the paleoceanographic significance of $^{231}Pa/^{230}Th$ data from Atlantic sediments is ongoing. For example, *Gherardi et al.* [2009] showed that similar depths in the North Atlantic Ocean display similar $^{231}Pa/^{230}Th$ at similar times, despite large differences in biogenic silica burial, and concluded that there were significant circulation changes during the deglaciation. *Peacock* [2010], however, questioned some aspects of this work, in particular the description of the modern MOC in the North Atlantic and the method of making composite vertical profiles of sediment $^{231}Pa/^{230}Th$ for various time slices from widely distant cores. *Gherardi et al.* [2010] replied that the data assembled in their previous study can best and most simply be explained by changes in ^{231}Pa export by the circulation. *Luo et al.* [2010] used a box model to argue that the relationship between sediment $^{231}Pa/^{230}Th$ at any given site and the meridional overturning circulation can be very complex. They claimed that constraining past changes in the MOC from $^{231}Pa/^{230}Th$ at one site is "impossible."

[10] Although past changes in particle composition may be an important control on sediment $^{231}Pa/^{230}Th$ [*Hall et al.*, 2006; *Gil et al.*, 2009; *Lippold et al.*, 2009], these changes remain poorly understood. For example, most of the biogenic silica produced in the sunlit layers of the ocean is dissolved in the water column or near the seafloor [e.g., *Nelson et al.*, 1995], suggesting that past changes in opal production may not be recorded in the sedimentary column. This state of affairs suggests that the interpretation of $^{231}Pa/^{230}Th$ data from deep-sea sediments involve significant uncertainties.

[11] Here an inverse method is used to investigate how (in)consistent sediment $^{231}Pa/^{230}Th$ data for distinct time intervals of the recent geologic past are with the abyssal circulation in the modern Atlantic Ocean. Earlier interpretations of these data are extended in three significant ways: (1) a model of the three-dimensional circulation is used, which is shown to be compatible with hydrographic observations and water column ^{231}Pa data, (2) earlier compilations of sediment $^{231}Pa/^{230}Th$ data are extended for each interval, and (3) the uncertainties arising from both limited data coverage and incomplete understanding of scavenging are given formal consideration. Note, however, that the major particulate phases carrying Pa in the ocean (e.g., opal) constitute an important issue that is not addressed here [e.g., *Siddall et al.*, 2005, and references therein].

[12] Our approach of data interpretation follows that of *LeGrand and Wunsch* [1995], *Gebbie and Huybers* [2006], and *Marchal and Curry* [2008]. First, an estimate of the modern circulation is obtained by combining observations with dynamical constraints. Second, the sediment data are adjusted to the modern circulation. If the adjustments to the data are generally larger than the data uncertainties, then compatibility of the sediment data with the modern circulation should be rejected.

[13] This paper is organized as follows. In section 2, the method used to estimate the abyssal circulation in the modern Atlantic Ocean and the sensitivity of the resulting solution to different assumptions are described. In section 3, a simple model of the transport of ^{231}Pa in the ocean is described. The consistency of water column ^{231}Pa data with our modern circulation estimate is tested. In section 4, the (in)compatibility of sediment $^{231}Pa/^{230}Th$ data for the Holocene, LGM, and H1 with the modern circulation and a hypothetical state of no flow is explored. The paleoceanographic implications of our results are discussed in section 5. Conclusions and perspectives follow in section 6.

2. Estimation of the Abyssal Circulation in the Modern Atlantic

2.1. Method

[14] An inverse method is used to provide an estimate of the abyssal circulation in the Atlantic Ocean, which is consistent with hydrographic data, observational estimates of volume transport at specific locations, and dynamical constraints. The model domain extends from 52°S to 60°N and from 1000 m to a maximum of 5000 m water depth (Figure 1). The model grid has a horizontal resolution of 4° × 4° and a vertical resolution of 1000 m. The model bathymetry is derived by averaging bathymetric data from ETOPO2 (National Geophysical Data Center, National Oceanic and Atmospheric Administration, U.S. Department of Commerce, ETOPO2v2 Global Gridded 2-minute Database, 2006, http://www.ngdc.noaa.gov/mgg/global/etopo2.html). Temperature, salinity, and pressure data from the hydrographic climatology of the World Ocean Circulation Experiment (WOCE [*Gourestki and Koltermann*, 2004]) are used to calculate in situ density at model grid points from the 1980 International Equation of State (note that model grid points coincide with points of the climatologic grid, so no interpolation is necessary). The standard deviations of temperature and salinity from WOCE climatology are propagated on the density uncertainty using a linear equation of state with $\partial\rho/\partial T = -2 \times 10^{-4}\ \rho_o$ kg m^{-3} °C^{-1} (ρ_o = 1028 kg m^{-3}) and $\partial\rho/\partial S = 0.8$ kg m^{-3}. For the error propagation, we assume no pressure error and no correlation between the temperature and salinity deviations.

Table 1. Prior Uncertainties to Estimate Modern Circulation

	Uncertainty (Sv)
Prior estimate of U, V, W	1
Volume conservation	0.01
Thermal wind (V)	1
Thermal wind (U)	1
Linear vorticity balance	1
NADW transport along western boundary	3
Integrated meridional transport at 36°N, 24°N, 32°S	3
AABW transport along western boundary in South Atlantic	1

[15] To further constrain the circulation, we consider observational estimates of the volume transport of (1) North Atlantic Deep Water (NADW) along the western boundary between 1000–4000 m (amplitude of 18 ± 3 Sv, where 1 Sv = 10^6 m^3 s^{-1} [*Schmitz and McCartney*, 1993]); (2) Mediterranean Outflow Water (MOW) at 12°W, between 32°N–36°N and 1000–2000 m (amplitude of 2 ± 0.3 Sv [*Ochoa and Bray*, 1991; *Baringer and Price*, 1997]); and (3) Antarctic Bottom Water (AABW) along the western boundary south of the equator between 4000–5000 m (amplitude of 7 ± 1 Sv [*Hogg et al.*, 1999; *Zenk et al.*, 1999]). The model bathymetry was deepened to 5000 m at four locations to accommodate a continuous flow path for AABW (e.g., through the Vema Channel). These locations correspond to grid boxes centered at: (50°S, 50°W), (30°S, 38°W), (26°S, 38°W), and (26°S, 34°W). We also rely on observational estimates to constrain the integrated meridional volume transport below 1000 m at three different latitudes. At 36°N and 24°N, the integrated transport is constrained to −20 ± 3 Sv, and at 32°S it is constrained to −15 ± 3 Sv, where the negative values imply a transport to the south [*Roemmich and Wunsch*, 1985; *Talley*, 2003; *Bryden et al.*, 2005].

[16] The dynamical constraints are the conservation of volume, the two thermal wind relationships, and the linear vorticity balance (see Appendix 1 in Text S1 in the auxiliary material).[1] The error for volume conservation is assumed to be 0.01 Sv, and the error for the thermal wind relationships and the linear vorticity balance is taken as 1 Sv. A summary of all of the prior uncertainties used to estimate the modern circulation can be found in Table 1. Note that the dynamical constraints are not imposed at all locations. The thermal wind relationships and the linear vorticity balance, which rely on the geostrophic approximation, are not prescribed between 4°S–4°N. Furthermore, the linear vorticity balance, which involves the meridional velocity, is not imposed at grid boxes with a meridional boundary or along the western boundary between 1000–4000 m.

[17] The modern circulation is estimated as a least squares solution which jointly satisfies the hydrographic data, the observational estimates of volume transport, and the dynamical constraints given their prior uncertainties [e.g., *Wunsch*, 1996]. A state vector, $\boldsymbol{x}$, is introduced that consists of the volume transports (U, V, W) defined on the faces of the grid boxes in the zonal, meridional, and vertical directions. A prior estimate of the state, $\boldsymbol{x_o}$, is determined by solving the thermal wind equations for U and V using the gridded densities from WOCE climatology and assuming a level of no motion at either 3000 m (as assumed in the inversion of *Martel and Wunsch* [1993]) or at 4000 m (approximately the boundary between NADW and AABW in the Brazil Basin, a relatively well studied abyssal basin [e.g., *Hogg and Owens*, 1999; *Morris et al.*, 2001]). If the local water depth is shallower than the assumed level of no motion, then the seafloor is taken as the level of no motion. After calculating U and V, W is obtained from volume conservation. The error covariance matrix of $\boldsymbol{x_o}$ is defined as $\boldsymbol{C_o} = \langle (\boldsymbol{x} - \boldsymbol{x_o})(\boldsymbol{x} - \boldsymbol{x_o})^{\mathrm{T}} \rangle$, where brackets denote the expected value and superscript T denotes the transpose. The diagonal elements of $\boldsymbol{C_o}$ are the variances of $\boldsymbol{x_o}$, and the off-diagonal elements are the error covariances. Thus, the diagonal elements of $\boldsymbol{C_o}$ are the squares of the uncertainty for the prior estimates of the transports (U, V, W), that is, $(1\ \mathrm{Sv})^2$ (Table 1).

[18] A system of linear algebraic equations, $\boldsymbol{Ax} + \boldsymbol{\varepsilon_A} = \boldsymbol{b}$, is derived from (1) the observational constraints on NADW transport along the western boundary and on the integrated meridional transport at 36°N, 24°N, and 32°S and (2) the finite difference forms of the dynamical equations. The matrix $\boldsymbol{A}$ includes the coefficients arising from the discretization of these differential equations on the model grid and the vector $\boldsymbol{b}$ includes the climatologic densities at the corners of the grid boxes. The error covariance matrix for this system is $\boldsymbol{C_A} = \langle (\boldsymbol{Ax} - \boldsymbol{b})(\boldsymbol{Ax} - \boldsymbol{b})^{\mathrm{T}} \rangle$. Thus, the diagonal elements of $\boldsymbol{C_A}$ are the squares of the uncertainties of the dynamical constraints (Table 1).

[19] Our problem is to find an estimate of $\boldsymbol{x}$ (i.e., a circulation) that satisfies both the observations and the dynamical constraints given their respective uncertainties. This estimate is provided by the minimum of the objective function:

$$\mathrm{J} = (\boldsymbol{x} - \boldsymbol{x_o})^{\mathrm{T}} \boldsymbol{C_o}^{-1} (\boldsymbol{x} - \boldsymbol{x_o}) + (\boldsymbol{Ax} - \boldsymbol{b})^{\mathrm{T}} \boldsymbol{C_A}^{-1} (\boldsymbol{Ax} - \boldsymbol{b}). \quad (1)$$

The first contribution to J represents the deviations from the prior estimate of the circulation. The second contribution represents the deviations from the observational estimates of volume transport and the deviations from the dynamical equations. Each contribution is weighted by its corresponding error covariance matrix. Here it is assumed that both $\boldsymbol{C_o}$ and $\boldsymbol{C_A}$ are diagonal, that is, there are no error covariances. If off-diagonal elements were retained in $\boldsymbol{C_o}$ and $\boldsymbol{C_A}$, the circulation estimate would be different (e.g., positive error correlations in $\boldsymbol{C_o}$ could lead to the estimation of more uniform distributions of U, V, and W).

[20] To find a minimum of J, the gradient $\frac{\partial J}{\partial \boldsymbol{x}}$ is set to zero, which leads to the system of linear algebraic equations

$$\left(\boldsymbol{C_o}^{-1} + \boldsymbol{A}^T \boldsymbol{C_A}^{-1} \boldsymbol{A}\right) \tilde{\boldsymbol{x}} = \boldsymbol{C_o}^{-1} \boldsymbol{x_o} + \boldsymbol{A}^T \boldsymbol{C_A}^{-1} \boldsymbol{b}. \quad (2)$$

Equation (2) is solved for $\tilde{\boldsymbol{x}}$ using LU decomposition. The vector $\tilde{\boldsymbol{x}}$ is the state estimate (circulation) at the minimum, that is, the solution of our problem. The uncertainty or error

[1] Auxiliary materials are available in the HTML. doi:10.1029/2010PA002022.

Table 2. Integrated Meridional Transports for the Modern Circulation Estimates

Latitude	Prior Transport (Sv)	Posterior Transport With Prior LNM at 3000 m[a] (Sv)	Posterior Transport With Prior LNM at 4000 m[a] (Sv)
36°N	−20 ± 3	−20 ± 8	−23 ± 8
24°N	−20 ± 3	−17 ± 8	−17 ± 8
32°S	−15 ± 3	−7 ± 7	−7 ± 7

[a]Posterior uncertainties are larger than the prior uncertainties because they are calculated from the individual transport uncertainties along the latitude line.

covariance matrix of the solution, $\mathbf{C} = \langle(\mathbf{x} - \tilde{\boldsymbol{x}})(\mathbf{x} - \tilde{\boldsymbol{x}})^{\mathrm{T}}\rangle$, is calculated by

$$\mathbf{C} = \left(\mathbf{E}^{\mathrm{T}}\mathbf{E}\right)^{-1}\mathbf{E}^{\mathrm{T}}\mathbf{C}_{\mathbf{oA}}\mathbf{E}\left(\mathbf{E}^{\mathrm{T}}\mathbf{E}\right)^{-1} \quad (3)$$

where $\boldsymbol{E} = \begin{bmatrix} \boldsymbol{I} \\ \boldsymbol{A} \end{bmatrix}$ is a partitioned matrix, $\mathbf{I}$ is the identity matrix, and $\boldsymbol{C_{oA}} = \begin{pmatrix} \boldsymbol{C_o} & 0 \\ 0 & \boldsymbol{C_A} \end{pmatrix}$.

2.2. Results

[21] We find that the circulations estimated with a prior level of no motion (LNM) at 3000 m or 4000 m are both consistent with hydrographic observations and dynamic constraints, given the uncertainties. For the solution with prior LNM = 3000 m, less than 5% of the elements of the state vector (U, V, W) differ from their prior values by more than two standard deviations (for easier reference these deviations are symbolically noted as $\sqrt{C_o}$) (Figure S1a in the auxiliary material). Likewise, less than 5% of the residuals in the dynamical constraints differ from zero by more than $\pm 2\sqrt{C_A}$ (Figure S1b). For the solution with prior LNM = 4000 m, similar results hold, although the largest normalized residuals $(\tilde{x} - x_o)/\sqrt{C_o}$ and $(A\tilde{x} - b)/\sqrt{C_A}$ are greater than for the solution with prior LNM = 3000 m (not shown). Both the solutions with prior LNM = 3000 m and 4000 m have posterior estimates of integrated meridional transports at 36°N, 24°N, and 32°S that are consistent with prior estimates (Table 2). Based on these results, only the solution (circulation) with prior LNM = 3000 m is chosen for the remainder of our study.

2.2.1. Circulation With Prior LNM at 3000 m

[22] Some elements of the estimated circulation with prior LNM at 3000 m are worth mentioning (Figures 2 and 3). The three upper layers of the model (1000–2000 m, 2000–3000 m, and 3000–4000 m) include a strong western boundary current (NADW). There are also intense zonal transports in the South Atlantic, which are associated with large meridional gradients of density. Additionally, the deepest layer shows a distinct northward flow along the western boundary in the Brazil Basin (AABW).

[23] The posterior uncertainties for the horizontal circulation between 2000–3000 m and 4000–5000 m are shown in Figures S2 and S3 in the auxiliary material. As expected, the posterior uncertainties are smaller than the prior uncertainties (Table 1). However, they remain comparable to the transport amplitudes in the interior (east of the western boundary), which are generally of the order of 1 Sv. The transports that are the best determined are along the western boundary between 1000–4000 m and in the southern South Atlantic, where transport amplitudes can reach up to 15 Sv in the shallowest layer (between 1000–2000 m). The integrated meridional transports at 36°N and 24°N are also relatively well determined (Table 2).

2.2.2. Sensitivity to Uncertainties

[24] The modern circulation is here estimated with different assumptions about the uncertainty for the prior state ($\boldsymbol{C_o}$). The uncertainty for the individual transports (U, V, W) is decreased from 1 Sv to 0.1 Sv and then to 0.01 Sv. We find that the decrease in uncertainty results in larger residuals for the observations and the dynamical equations, even though the fraction of residuals larger than $2\sqrt{C_o}$ (in absolute magnitude) remains less than 5% (Table 3). For an uncertainty of 0.01 Sv, the integrated flow at 24°N and 36°N is reduced in amplitude, and the flow at 32°S is northward (Table 3). The decrease in meridional transport amplitude results from the increased confidence in the prior circulation, which is determined by the density differences via the thermal wind relationships. These density differences are

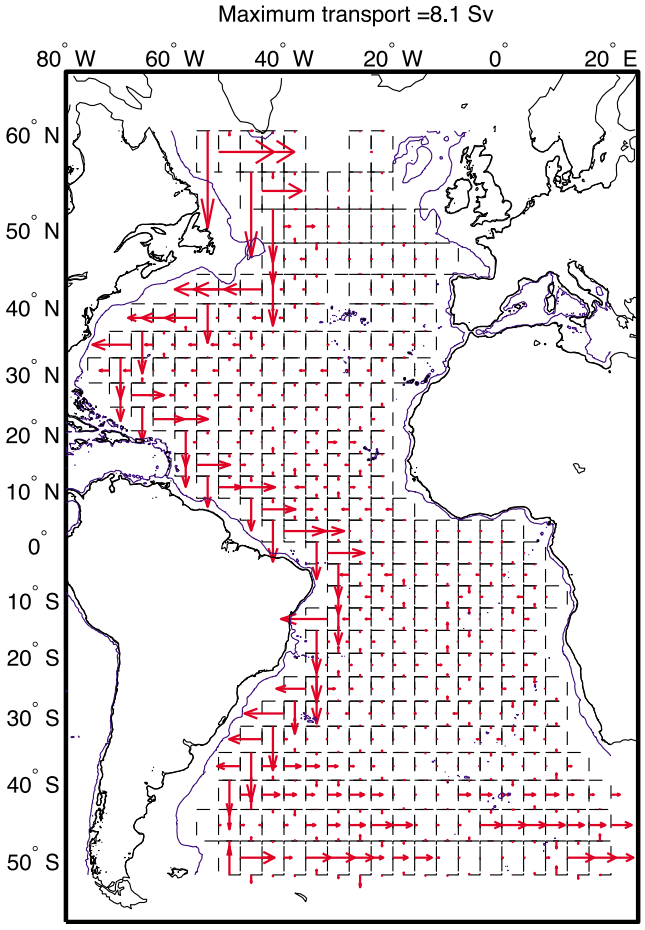

Figure 2. Horizontal circulation between 2000 and 3000 m (solution with prior LNM at 3000 m). Red vectors are volume transports, with a maximum transport of about 8.1 Sv. The blue line is the 1000 m isobath. The grid is the model grid.

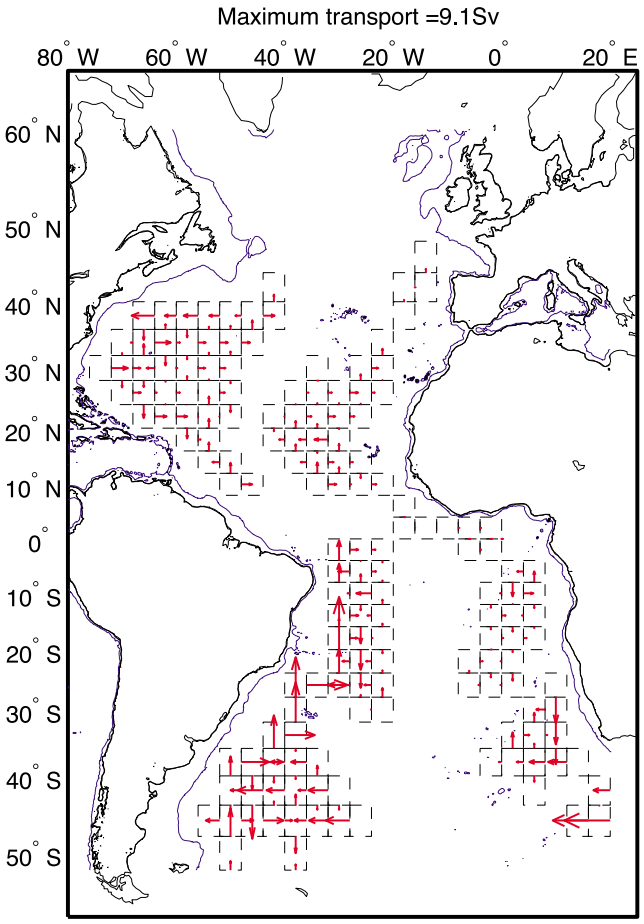

Figure 3. Same as Figure 2 but for circulation between 4000–5000 m.

very small at most locations, especially in the interior of the basin, which results in small volume transports.

[25] The modern circulation is then estimated with different assumptions about the uncertainty in the dynamical constraints ($\boldsymbol{C_A}$). The uncertainty of the geostrophic approximation (thermal wind relationships and linear vorticity balance) is reduced from 1 Sv to 0.1 Sv and then to 0.01 Sv. As this uncertainty is decreased, the fraction of residuals greater than $2\sqrt{C_A}$ increases (Table 4). As the uncertainty for geostrophy decreases to 0.01 Sv, the integrated meridional transports decrease in amplitude (Table 4). The decreased uncertainty in geostrophy places a greater emphasis on the small density gradients in the interior of the basin, thus resulting in reduced meridional transport.

[26] Given the difficulty in providing error estimates for the prior circulation ($\mathbf{C_o}$) and for geostrophic dynamics in the abyssal ocean ($\mathbf{C_A}$), the quantitative elements of our solution should be interpreted with caution. Such a solution, however, will be useful for examining the (in)consistency with the modern circulation of ^{231}Pa observations from the water column and ^{231}Pa/^{230}Th observations from the sediment.

3. Analysis of Water Column ^{231}Pa Data

3.1. Data

[27] Measurements of dissolved, particulate, and total ^{231}Pa activity in the abyssal Atlantic Ocean (water depths greater than or equal to 1000 m) are compiled (Table 5). According to our compilation, dissolved, particulate, and total ^{231}Pa activity have been measured on water samples collected at 23, 12, and 18 stations, respectively. Our compilation comprises a total number of 236 measurements of dissolved or total ^{231}Pa activity at 32 stations, where the number of measurements per station ranges from 2 to 14. The data coverage is poor and uneven (Figure 1).

3.2. Advection-Scavenging Model

[28] In order to gauge the (in)consistency of water column ^{231}Pa data with a given circulation state, a model describing the behavior of ^{231}Pa in the ocean is necessary. Here, the reversible exchange model [*Nozaki et al.*, 1981; *Bacon and Anderson*, 1982] is extended to include the effect of advection of ^{231}Pa by the circulation. Thus, the governing equations for dissolved ($[Pa]_d$) and particulate ^{231}Pa activity ($[Pa]_p$) in the ocean are

$$\vec{u} \cdot \nabla [Pa]_d = \beta_{231} + k_d [Pa]_p - k_a [Pa]_d + \varepsilon_d \qquad (4)$$

and

$$\vec{u} \cdot \nabla [Pa]_p + w \frac{\partial [Pa]_p}{\partial z} = k_a [Pa]_d - k_d [Pa]_p + \varepsilon_p, \qquad (5)$$

respectively. Here $\vec{u}$ is the fluid velocity, $\beta_{231} = 2.4 \times 10^{-3}$ dpm m^{-3} y^{-1} is the production of ^{231}Pa from radioactive decay of ^{235}U [*Scholten et al.*, 1995], k_d (k_a) is the desorption (adsorption) rate constant for ^{231}Pa off/onto particles, w is the sinking velocity of particles that participate in scavenging of Pa, and (ε_d, ε_p) are errors stemming from various approximations in equations (4) and (5). Summing (4) and (5) gives a governing equation for the

Table 3. Sensitivity Tests on the Uncertainty in the Prior Circulation

Prior Uncertainty in U,V,W (Sv)	Adjustments of U,V,W Greater Than or Less Than $2\sqrt{C_o}$ (%)	Linear Constraint Residuals Greater Than or Less Than $2\sqrt{C_A}$ (%)	Posterior Transport at 36°N (Sv)	Posterior Transport at 24°N (Sv)	Posterior Transport at 32°S (Sv)
1	0.9	1.5	−20 ± 8	−17 ± 8	−7 ± 7
0.1	1.1	3.3	−15 ± 2	−10 ± 1	3 ± 1
0.01	1.1	3.3	−8 ± 0.5	−3 ± 0.2	9 ± 0.2

Table 4. Sensitivity Tests on the Uncertainty in the Geostrophic Approximation

Uncertainty (Sv)	Adjustments of U,V,W Greater Than or Less Than $2\sqrt{C_o}$ (%)	Linear Constraint Residuals Greater Than or Less Than $2\sqrt{C_A}$ (%)	Posterior Transport at 36°N (Sv)	Posterior Transport at 24°N (Sv)	Posterior Transport at 32°S (Sv)
1	0.9	1.5	−20 ± 8	−17 ± 8	−7 ± 7
0.1	5.6	2.8	−17 ± 7	−13 ± 6	−0.8 ± 5
0.01	6.6	8.4	−16 ± 7	−13 ± 6	−0.1 ± 5

activity of total ^{231}Pa, [Pa] = $[Pa]_d$ + $[Pa]_p$. Introducing the partition parameter $k_{Pa} = [Pa]_p/[Pa]$, this equation becomes

$$\vec{u} \cdot \nabla [Pa] + w\frac{\partial}{\partial z}([Pa]k_{Pa}) = \beta_{231} + \varepsilon. \quad (6)$$

Thus, the transport of total ^{231}Pa by advection and sinking particles is balanced locally by the production of ^{231}Pa from the radioactive decay of ^{235}U within an error ε.

3.3. Scavenging Parameters

[29] The advection-scavenging model (6) includes two parameters (w and k_{Pa}). The sinking velocity (w) is based on published estimates determined from the vertical distribution of particulate ^{230}Th measured at stations in the Indian and Atlantic oceans [*Krishnaswami et al.*, 1976; *Krishnaswami et al.*, 1981; *Rutgers van der Loeff and Berger*, 1993; *Scholten et al.*, 1995; *Venchiarutti et al.*, 2008]. A value of 750 m yr^{-1} is assumed. Whereas this choice is somewhat arbitrary, it is within the range of values (300–900 m yr^{-1}) reported in these studies.

[30] The partitioning of Pa between particulate and dissolved forms (as expressed by $k_{Pa} = [Pa]_p/[Pa]$) is expected to vary in the ocean owing to variations in particle concentration and particle composition. Consider the defining relation

$$\frac{[Pa]_p}{[Pa]} \equiv K_d C_p, \quad (7)$$

where C_p is the concentration of particles (mass of particles/mass of seawater) and K_d is a "pseudo-Kd" partition coefficient [*Chase et al.*, 2002]. Our knowledge about the distribution of suspended particulate matter at abyssal depths in the Atlantic Ocean stems primarily from direct measurements by filtration [e.g., *Brewer et al.*, 1976] or from observations of light scattering or attenuation [e.g., *Biscaye and Eittreim*, 1977]. Whereas optical measurements are more abundant, uncertainties remain in their conversion to particle concentration [e.g., *Bishop*, 1999, and references therein]. Nevertheless, both direct and optical measurements indicate that the bottom waters of the western Atlantic generally exhibit large turbidity levels (bottom nepheloid layer) [*Brewer et al.*, 1976; *Biscaye and Eittreim*, 1977]. Optical observations reveal that turbidity is particularly elevated near the western boundary [*Biscaye and Eittreim*, 1977].

[31] Based on these observations, we assume that the fraction of ^{231}Pa in particles (k_{Pa}) is larger near the western boundary than in the interior. The k_{Pa} value assigned at grid boxes adjacent to the western boundary is based on paired measurements of particulate and total ^{231}Pa activity (k_{Pa}) within 300 m of the seafloor at three stations within the domain: (58.19°N, 50.87°W) [*Moran et al.*, 2002], (44.48°S, 10.46°E) [*Rutgers van der Loeff and Berger*, 1993], and (33°S, 40°W) [*Moran et al.*, 2001] (Figure S4a). At each of these stations, k_{Pa} measured within 300 m of the seafloor is much larger than values measured at shallower depths, which likely results from higher concentration of suspended particles in the bottom nepheloid layer. Here k_{Pa} in the western boundary is set equal to 0.12, which is the average k_{Pa} measured within 300 m of the seafloor at these stations.

[32] To constrain k_{Pa} east of the western boundary, we consider again paired measurements of particulate and total ^{231}Pa activity in the water column. Paired measurements from 12 stations in the Atlantic Ocean do not reveal a general dependence of k_{Pa} on depth below 1000 m (Figure S4a). A statistical test based on a rank correlation coefficient [e.g., *Kendall and Gibbons*, 1990] indicates no significant monotonic variation of k_{Pa} with depth (all p values greater than 0.05), with the exception of three stations with a significant increase (58.19°N, 50.87°W; 0.59°S, 20.03°W; 17°S, 25°W) and one with a significant decrease (25°S, 3.48°E). On the other hand, the depth-averaged k_{Pa} at stations where paired ^{231}Pa data are available do suggest a latitudinal dependence, with higher values occurring south of 40°S (Figure S4b). The high values of k_{Pa} observed at four stations south of this latitude likely reflect the presence of biogenic opal [e.g., *Walter et al.*, 1997, 2001]. Here, in the abyssal region east of the western boundary and south of 40°S, k_{Pa} is set equal to 0.08, which is the average k_{Pa} for these stations (n = 10). In the abyssal region east of the western boundary and north of 40°S, k_{Pa} is set equal to 0.02, which is the average k_{Pa} for stations north of this latitude (n = 53). Clearly, more paired ^{231}Pa measurements are needed to better constrain spatial variations of k_{Pa} in the Atlantic Ocean, especially in the northern hemisphere where such measurements are critically lacking.

[33] Finally, the error term (ε) in the governing equation for total ^{231}Pa (6) should not be negligible as it accounts for

Table 5. Measurements of Water Column ^{231}Pa Activity Used in This Study

Reference	Dissolved	Particulate	Total
Rutgers van der Loeff and Berger [1993]	x	x	x
Moran et al. [2001, 2002]	x	x	x
Scholten et al. [2008]		x	x
Luo et al. [2010]	x		
R. François (unpublished data, 2005)	x		

various approximations in (6), such as the assumption of steady state, the omission of mixing by eddies, and the assumptions of the reversible exchange model. The lack of an explicit representation by eddy mixing [see also *LeGrand and Wunsch*, 1995; *Huybers et al.*, 2007; *Marchal and Curry*, 2008] and other model limitations are discussed in section 5.3. In order to account for the significant uncertainties in (6), it is assumed that ε can be of the same order as the production rate β_{231}. Since ^{231}Pa production appears as a first-order term in the basin-scale balance of the tracer [e.g., *Yu et al.*, 1996], this assumption is likely conservative.

3.4. Inverse Method

[34] An inverse method identical to that employed in section 2.2 is used to determine how (in)consistent water column measurements of total ^{231}Pa activity, [Pa], are with (1) our modern circulation estimate and (2) a hypothetical state of no flow (with no advection). A system of linear algebraic equations, $\boldsymbol{Gx} + \boldsymbol{\varepsilon_G} = \boldsymbol{h}$, is derived from the finite difference form of equation (6) (see Appendix 1 in Text S1), where $\boldsymbol{G}$ includes the coefficients arising from the discretization of (6), $\boldsymbol{x}$ is the state vector with [Pa] at the grid box centers, $\boldsymbol{h}$ is a source term proportional to β_{231}, and $\boldsymbol{\varepsilon_G}$ is an error. For consistency test 1, $\boldsymbol{G}$ includes the individual volume transports (U,V,W) estimated in section 2.2 (with a prior LNM = 3000 m), whereas for 2, $\boldsymbol{G}$ is constructed with U = V = W = 0. For both cases, $\boldsymbol{C_G} = \langle(\boldsymbol{Gx} - \boldsymbol{h})(\boldsymbol{Gx} - \boldsymbol{h})^{\mathrm{T}}\rangle$ is taken as diagonal (no error covariances).

[35] An objective function of the same form as equation (1) is minimized, leading again to a linear problem of the type in equation (2). Here the vector $\boldsymbol{x_o}$ includes a prior estimate of the distribution of [Pa] in the deep Atlantic ([Pa] at the center of model grid boxes), and $\boldsymbol{C_o} = \langle(\boldsymbol{x} - \boldsymbol{x_o})(\boldsymbol{x} - \boldsymbol{x_o})^{\mathrm{T}}\rangle$ is the error covariance matrix for this estimate. Both $\boldsymbol{x_o}$ and $\boldsymbol{C_o}$ are determined from water column [Pa] data at 32 stations in the Atlantic Ocean (Figure 1) using objective mapping [e.g., *Bretherton et al.*, 1976]. At some of these stations, only $[\mathrm{Pa}]_\mathrm{d}$ has been measured (Figure 1, open triangles). They are converted to [Pa] assuming the average $k_{Pa} = 0.03$ (n = 61) determined from all available paired ^{231}Pa observations in the deep Atlantic (section 3.3). Although a spatially varying k_{Pa} would be more appropriate, the average k_{Pa} is used here for simplicity given the small correction (i.e., most ^{231}Pa is present in dissolved form). Three parameters are required for objective mapping: a horizontal scale (L_H) measuring the covariance between [Pa] at different geographic locations, a vertical scale (L_Z) measuring the covariance between [Pa] at different depths, and the maximum variance of [Pa] at locations infinitely far from data locations (r_0) [*Marchal et al.*, 2007]. Here we assume that the covariance between [Pa] at two locations drops exponentially with $L_H = 10^6$ m and $L_Z = 10^3$ m, which are comparable to values assumed in earlier work for mapping the distribution of ^{230}Th [*Marchal et al.*, 2007]. The maximum variance is set equal to 0.017 (dpm m^{-3})^2, which is the variance of [Pa] measurements in the deep Atlantic (Table 5).

[36] The objective mapping of [Pa] based on these parameter values is assessed a posteriori by comparing the mapped [Pa] at data locations with the measured [Pa] (Figure S5). We find that all of the mapped [Pa] values are within two standard deviations of the measured values, indicating that the mapping is consistent with the existing set of water column [Pa] data. Note that far from data locations the mapped [Pa] tends to the average of the [Pa] measurements and its uncertainty tends to the relatively large value $\sqrt{r_0}$. Thus far from data locations, the mapping leads to considerable smoothing (with large uncertainties in mapped [Pa]) and does not elucidate high tracer gradients which may be present in reality.

[37] The objectively mapped distributions of [Pa] and of its uncertainty in the deep Atlantic (z = 1500 m) are displayed in Figure 4. There is a general increase in [Pa] from north to south (Figure 4a). Zonal variations in [Pa] are present as well, in particular in the South Atlantic where measurements in the Angola and Cape basins [*Scholten et al.*, 2008] appear particularly large. As expected, the uncertainties in [Pa] are smallest near data locations and increase with distance from these locations (Figure 4b).

[38] Our analysis of [Pa] data in the deep Atlantic requires knowledge of [Pa] near the open lateral boundaries (52°S; 60°N; 20°E for latitudes south of 40°S; and at 12°W between 32°N–36°N for MOW) and the upper boundary (z = 1000 m); such requirement arises from the definition of [Pa] at the center of grid boxes (see Appendix 1 in Text S1). The [Pa] values near the lateral boundaries are derived from objective mapping as described above. The activity of total ^{231}Pa at 500 m is estimated from [Pa] measurements in the upper 1000 m in the Atlantic Ocean. These measurements suggest a linear trend with depth (not shown), consistent with a reversible exchange with particles. A linear regression of these data with depth gives a slope of $(2.14 \pm 0.35) \times 10^{-4}$ dpm m^{-4} and an intercept of (0.057 ± 0.016) dpm m^{-3} (n = 32). The [Pa] value at 500 m obtained from this regression is 0.164 dpm m^{-3}, which provides the upper boundary condition.

[39] Finally, the uncertainty in the discretized form of the advection-scavenging model is set equal to the production rate of ^{231}Pa integrated over the volume of the grid box, that is, $\sqrt{C_G} = \beta_{231}\mathrm{V}$, which is equal to about 10^4 dpm s^{-1}. As stipulated above, this assumption is probably conservative. The sensitivity of the results to the boundary condition at z = 500 m and to the assumptions about objective mapping (L_H, L_Z, r_0) is examined in section 3.5.

3.5. Results

[40] The (in)consistency of the water column [Pa] data with the two circulation schemes (modern circulation and state of no flow) is measured by the normalized adjustment or residual, $(\tilde{x} - x_o)/\sqrt{C_o}$, at the grid points near data locations (n = 83, where n is the number of grid points near [Pa] data). These adjustments are nondimensional and represent the deviations from the original, objectively mapped [Pa] values (x_o) divided by the standard deviations of these values ($\sqrt{\mathrm{C_o}}$). Thus an adjustment of $+2\sqrt{\mathrm{C_o}}$ ($-2\sqrt{\mathrm{C_o}}$) at a given location means that the ^{231}Pa activity at that location as estimated by objective mapping must be increased (decreased) by two times its standard deviation to be consistent with the circulation scheme.

[41] We find that 8% of [Pa] values near data locations are modified by more than $2\sqrt{\mathrm{C_o}}$ to reach consistency with the

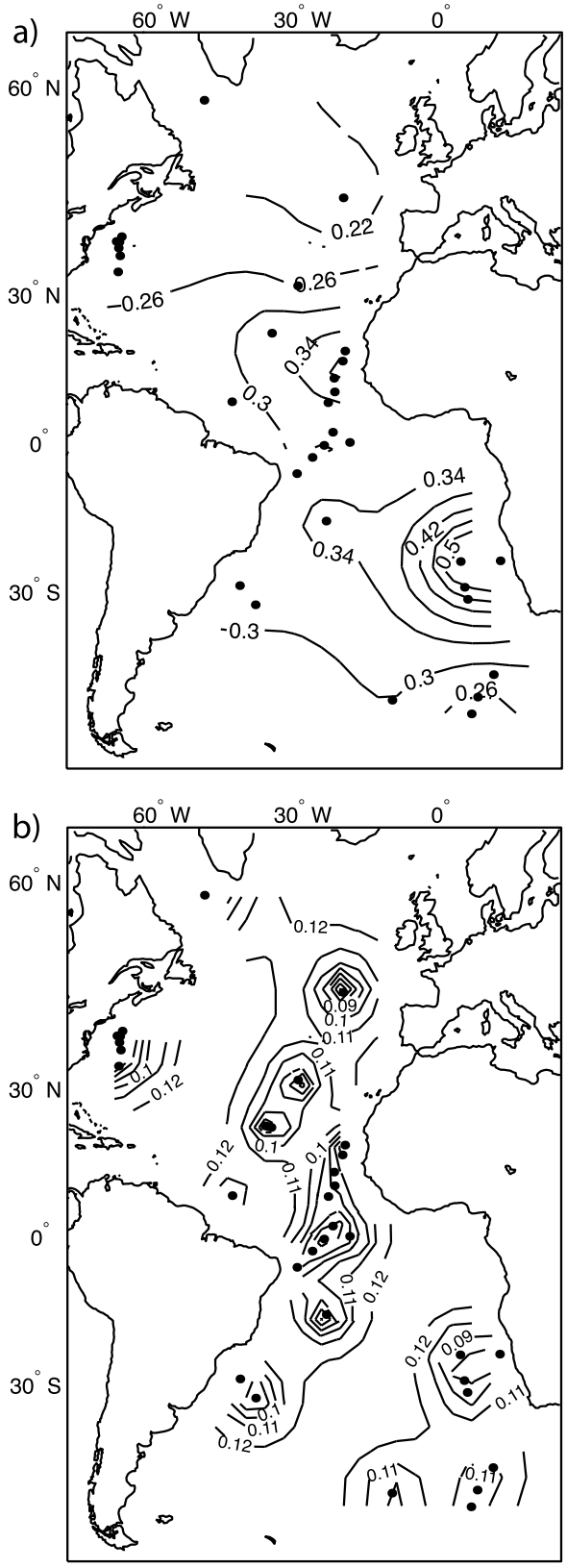

modern circulation, as compared to 34% for the state of no flow (Figure 5). The [Pa] adjustments needed to comply with the modern circulation show a geographic pattern. All six of the negative residuals which are more negative than $-2\sqrt{C_o}$ occur in the eastern South Atlantic (Figure 1). As mentioned above, compared to other locations in the Atlantic Ocean, [Pa] measurements from the eastern South Atlantic [*Scholten et al.*, 2008] have the highest values (Figure 4a). Strong negative adjustments are needed to bring these measurements into consistency with our estimate of the modern circulation.

[42] The adjustments needed to bring the [Pa] values near data locations into consistency with the modern circulation are skewed toward negative, with an average residual of −0.51. When the measurements from the eastern South Atlantic [*Scholten et al.*, 2008] are excluded from the analysis, the average residual becomes −0.16. In contrast, the adjustments to a state of no flow (average = 1.24 considering all measurements) show a strong positive bias that increases with depth. Positive residuals imply that the [Pa] observations are too low to be explained without advection. The positive bias is expected because a reversible exchange of ^{231}Pa without any advection would require a linear increase of [Pa] with depth, that is, relatively large [Pa] in deep water. In the modern Atlantic, [Pa] in deep water is generally lower than predicted by pure reversible exchange, and this offset is larger at greater depths [e.g., *Moran et al.*, 2002; *Luo et al.*, 2010]. Thus, large positive adjustments in deep water (increases in the objectively mapped [Pa] data) are generally needed to bring the water column [Pa] data into consistency with a state of no flow.

[43] The above results appear to be essentially independent of the boundary value of [Pa] at 500 m water depth. Increasing (decreasing) [Pa] at 500 m by a factor of two results in only 7% (12%) of the [Pa] values near data locations being modified by more than $2\sqrt{C_o}$ to reach consistency with the modern circulation, as compared to 61% (37%) for the state of no flow.

[44] On the other hand, the above results are sensitive to some of the parameters assumed in the objective mapping of [Pa] in the Atlantic Ocean. Generally, it is expected that lower values of (L_H, L_Z) and higher values of r_0 lead to higher uncertainties in the mapped distribution. Consider first the variance r_0, which above was set equal to the variance of the [Pa] measurements in the Atlantic Ocean. If r_0 is taken instead as half of the range of these measurements, only 2 out of the 83 [Pa] values (2%) near data locations need to be modified by more than $2\sqrt{C_o}$ to comply with our modern circulation estimate, compared to only 10 out of 83 (12%) for the state of no flow (if r_0 is equal to the variance in [Pa] measurements, we found that those numbers are 7

Figure 4. (a) Distribution of total ^{231}Pa activity, [Pa], at 1500 m water depth determined by objective mapping. Contour interval is 0.04 dpm m^{-3}. (b) Distribution of the uncertainty of [Pa] (dpm m^{-3}) at 1500 m water depth determined by objective mapping. Contour interval is 0.01 dpm m^{-3}. Station locations are indicated by dots.

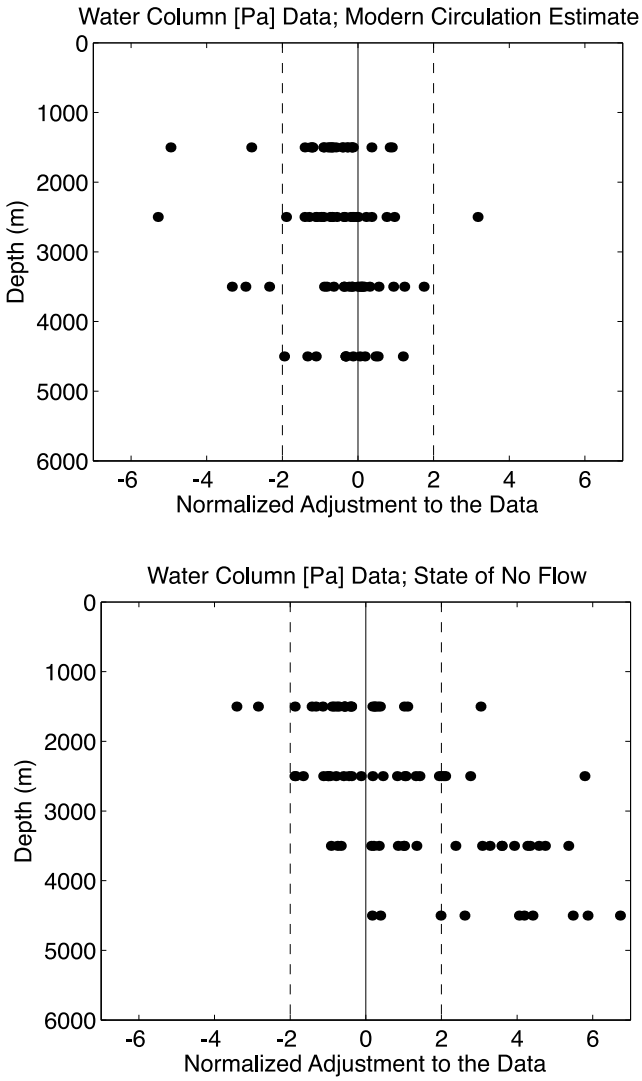

Figure 5. Adjustments of water column ^{231}Pa activity to (top) the modern circulation or (bottom) a hypothetical state of no flow. The adjustments are normalized to uncertainties. The dashed lines represent the $2\sqrt{C_o}$ band.

and 28 (8% and 34%), respectively). As expected, when the uncertainties in the tracer distribution are increased, the tracer data become more consistent with a given circulation scheme, and it becomes more difficult for these data to distinguish between different circulations.

[45] A similar effect is observed by decreasing the length scale L_H. If L_H is decreased by a factor of two (hence reducing the correlation between tracer values at different geographic locations), slightly more of the [Pa] values near data locations appear consistent with the modern circulation (state of no flow); only 6 (24) of the 83 adjustments (7% or 29%, respectively) exceed $2\sqrt{C_o}$ in absolute magnitude. Decreasing L_Z by a factor of two (reducing the correlation between tracer values at different depths) does not change the percentage consistent with either circulation scheme.

[46] In summary, most measurements of [Pa] in the Atlantic Ocean can be brought into consistency with the modern circulation if plausible assumptions are made about the [Pa] distribution and model uncertainties. The level of consistency is largely insensitive to the boundary value of [Pa] at 500 m, but is sensitive to some of the assumptions made in the objective mapping. In all cases, however, the [Pa] measurements are less consistent with the state of no flow, indicating that advection is needed to explain the modern water column data.

4. Analysis of Sediment ^{231}Pa/^{230}Th Data

4.1. Data

[47] The ^{231}Pa/^{230}Th data for the Holocene (core tops) and Last Glacial Maximum (LGM) come from a total of 39 cores (Figure 1). While there are additional cores with Holocene ^{231}Pa/^{230}Th data that are used to evaluate the conversion of ^{231}Pa/^{230}Th to [Pa] (see section 4.3.1), only those cores that have both LGM and Holocene ^{231}Pa/^{230}Th are considered for analysis. Data from twenty-seven of these cores come from the thesis of *Yu* [1994]. For the other twelve cores, data come either from more recent studies [*McManus et al.*, 2004; *Gherardi et al.*, 2005; *Hall et al.*, 2006; *Bradtmiller et al.*, 2007; *Gherardi et al.*, 2009] or are unpublished (L. Bradtmiller, unpublished data, 2009). For these twelve cores, Holocene is defined as the time interval 0–6 kyr B.P. and LGM is defined as the time interval 18–21 kyr B.P., as by *Gherardi et al.* [2005]. For each core, the average of the ^{231}Pa/^{230}Th data within those intervals is used, and the uncertainty is taken as the larger of (1) the average of the uncertainties reported for those data points within the interval and (2) the standard error of the ^{231}Pa/^{230}Th values within the interval.

[48] The ^{231}Pa/^{230}Th data for the Heinrich Event 1 (H1) from fifteen cores are used [*McManus et al.*, 2004; *Gherardi et al.*, 2005; *Hall et al.*, 2006; *Bradtmiller et al.*, 2007; *Gherardi et al.*, 2009]. For four of these cores, unpublished data are provided by L. Bradtmiller (unpublished data, 2009). All fifteen cores are from the north and equatorial Atlantic (Figure 1). H1 is defined as the time interval 15–17 kyr B.P., as by *Gherardi et al.* [2005], and the averages and uncertainties are calculated as for the LGM values.

4.2. Conversion of ^{231}Pa/^{230}Th Into [Pa]

[49] The inverse method described in section 3.4 is used to test the (in)consistency of Holocene, LGM, or H1 ^{231}Pa/^{230}Th observations with both the modern circulation and a state of no flow. To this end, the activity of total ^{231}Pa in bottom water at the core location is estimated from ^{231}Pa/^{230}Th in the sediment:

$$[Pa] = \frac{[Pa]_p}{k_{Pa}} = \frac{1}{k_{Pa}} \left(\frac{^{231}Pa}{^{230}Th} \right)_{sed} [Th]_p. \quad (8)$$

Here k_{Pa} is the partition parameter introduced in section 3.2, (^{231}Pa/^{230}Th)$_{sed}$ is the radionuclide ratio in the sediment, and [Th]$_p$ is the activity of particulate ^{230}Th in bottom water (in dpm m^{-3}). Thus, provided that an estimate of k_{Pa} and [Th]$_p$ is available, [Pa] can be reconstructed from the sediment ^{231}Pa/^{230}Th.

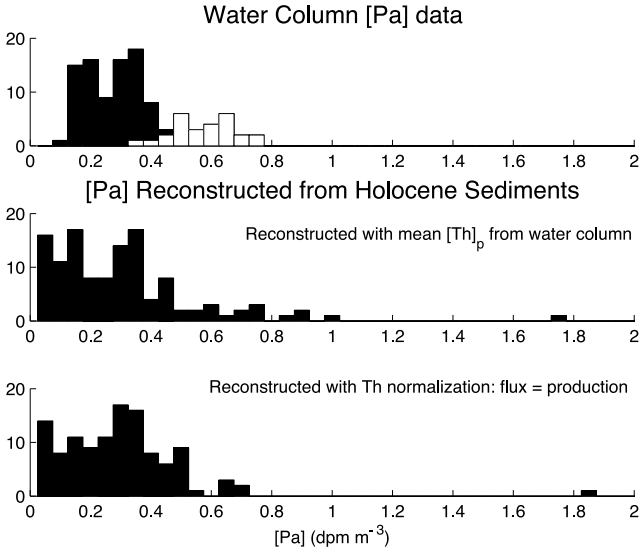

Figure 6. Frequency distribution of the water column [Pa] data (z > 1000 m) for 18 stations in the Atlantic Ocean (data from *Scholten et al.* [2008] are in white) compared to the frequency distribution of bottom water [Pa] reconstructed from Holocene sediment $^{231}Pa/^{230}Th$ estimated using either (1) mean $[Th]_p$ from water column data or (2) $[Th]_p = \beta_{230}z/w$ (see text).

[50] The partition k_{Pa} used in (8) is the spatially variable distribution based on paired water column data (section 3.3). On the other hand, two different approaches are used to estimate $[Th]_p$. First, $[Th]_p$ is set equal to the average of all water column measurements of $[Th]_p$ at depths greater than 1000 m in the Atlantic Ocean [*Rutgers van der Loeff and Berger*, 1993; *Moran et al.*, 2001; *Moran et al.*, 2002; *Scholten et al.*, 2008]. Based on the limited $[Th]_p$ data available, no obvious geographic trend of $[Th]_p$ is apparent (Figure S4c), justifying our approach of using an average value for $[Th]_p$. This average in the Atlantic Ocean amounts to 0.113 dpm m^{-3} (n = 77). The second approach assumes that the flux of scavenged ^{230}Th to the sediment is equal to the production of ^{230}Th in the water column overlying the sediment. This assumption is at the core of the "^{230}Th normalization method," which relies on ^{230}Th measurements in the sediment to correct apparent downcore changes in the vertical flux of material for the effects of lateral sediment redistribution [*François et al.*, 2004]. Thus, $[Th]_p$ is derived from the following relationship

$$[Th]_p w = \beta_{230} z. \tag{9}$$

Here w is the sinking velocity of the particles that scavenge ^{230}Th, β_{230} is the production rate of ^{230}Th, and z is the water depth of the sediment core. The activity, $[Th]_p$, is obtained from equation (9), assuming $w = 750$ m yr^{-1} (section 3.3) and $\beta_{230} = 2.67 \times 10^{-2}$ dpm m^{-3} yr^{-1} [e.g., *Cheng et al.*, 2000].

[51] The propagated error for bottom water [Pa] at core locations reconstructed from (8) using $[Th]_p$ measurements or the normalization method (9) only takes into account the uncertainty of $^{231}Pa/^{230}Th$ measurements, leading to an underestimation of the total error. This assumption is motivated by (1) the fact that the uncertainties of parameters such as w and k_{Pa} are difficult to estimate for the past and (2) our willingness to give sediment $^{231}Pa/^{230}Th$ data the best chance to reject consistency with the modern circulation.

[52] Estimates of total ^{231}Pa activity and of its uncertainty at the centers of model grid boxes are derived from bottom water [Pa] at core locations using objective mapping (section 3.4). For all three sediment data sets (Holocene, LGM, and H1), less than 3% of the mapped [Pa] values at core locations are greater or less than two standard deviations from the reconstructed [Pa] values, indicating that the mapping parameters are consistent with the reconstructed values. The mapped [Pa] values are assigned to the prior state ($\boldsymbol{x_o}$), and their variances and error covariances are assigned to the error covariance matrix ($\boldsymbol{C_o}$).

4.3. Results

4.3.1. Comparison of Holocene and Water Column [Pa]

[53] It is instructive to compare the bottom water [Pa] at core locations reconstructed from Holocene (core top) sediments with the direct measurements of [Pa] in the water column, even though these do not occur at the same geographic locations. For this comparison, we consider (1) all 121 cores within the domain that have Holocene $^{231}Pa/^{230}Th$ data (for a list of references see Appendix 2 in Text S1 in the auxiliary material) and (2) measurements of total (dissolved + particulate) ^{231}Pa activity at depths greater than 1000 m in the Atlantic Ocean (109 measurements at eighteen stations). The frequency distribution of the water column measurements is compared with the frequency distribution of the reconstructed bottom water [Pa] from the Holocene $^{231}Pa/^{230}Th$ data using the two methods of estimating $[Th]_p$ described in section 4.2 (Figure 6).

[54] The frequency distributions of both measured [Pa] and reconstructed [Pa] suggest the presence of more than one mode in their respective underlying distributions. The presence of several modes suggests that a classical (parametric) statistical procedure would not be appropriate for testing differences between the distributions of measured and reconstructed [Pa], since such procedures typically assume that the underlying distributions are Gaussian or normal (i.e., unimodal). Here, a nonparametric procedure, which makes weaker assumptions about the underlying distributions, is used to test such differences. A Mann-Whitney-Wilcoxon test suggests that the measured [Pa] values and the [Pa] values reconstructed from $(^{231}Pa/^{230}Th)_{sed}$ do not come from the same underlying distributions using either the average observed $[Th]_p$ or the $[Th]_p$ calculated from (9) ($p = 0.01$ and 0.03, respectively). As mentioned previously, the water column [Pa] data from the eastern South Atlantic [*Scholten et al.*, 2008] are high compared to data from other areas in the Atlantic Ocean. These data could bias the frequency distribution of water column [Pa] measurements toward high values since they make up 25% of the water column data set (in contrast $(^{231}Pa/^{230}Th)_{sed}$ measurements from the eastern South Atlantic constitute only 15% of our sediment data set). When water column and sediment data from the eastern South Atlantic are disregarded, the frequency distributions

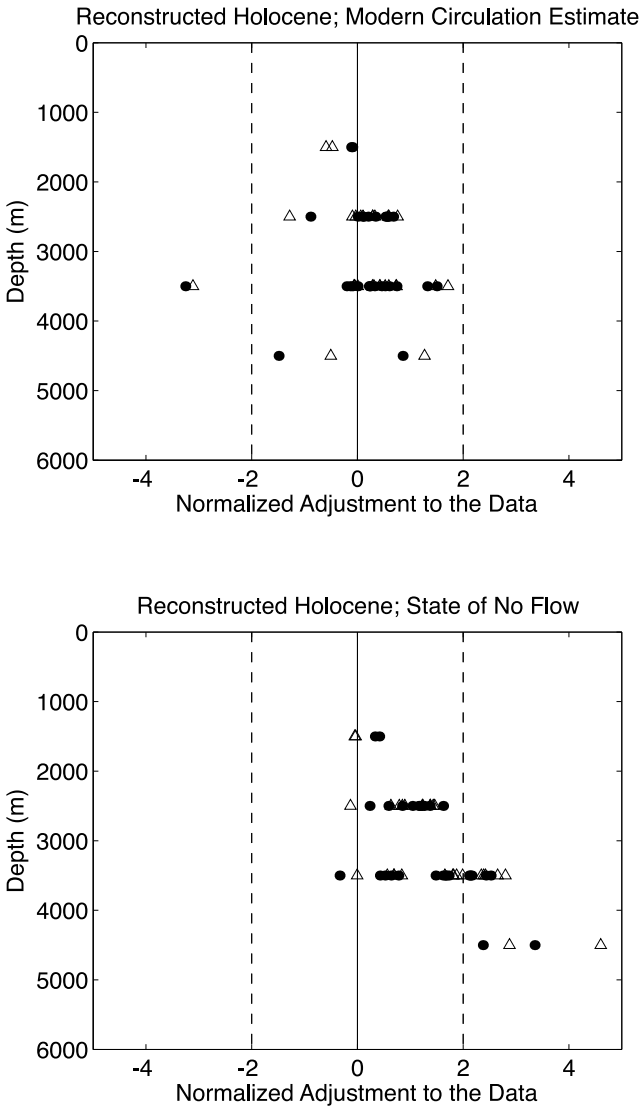

Figure 7. Adjustment of reconstructed ^{231}Pa activity in bottom water near core locations during the Holocene to (top) the modern circulation and (bottom) a hypothetical state of no flow. The ^{231}Pa activity is reconstructed from sediment ^{231}Pa/^{230}Th assuming (1) mean $[Th]_p$ from water column data (open triangle) or (2) $[Th]_p = \beta_{230}z/w$ (filled circle). In both panels the adjustments are normalized to the uncertainties.

of reconstructed [Pa] appear no longer different from the frequency distribution of measured [Pa] (p = 0.26 and 0.71 for the two approaches to estimate $[Th]_p$). Since there are apparent differences in the frequency distribution of [Pa] reconstructed using the two different approaches for estimating $[Th]_p$, each analysis is done twice, once with each approach.

4.3.2. Test of Consistency of Sediment ^{231}Pa/^{230}Th

[55] To test the consistency of sediment ^{231}Pa/^{230}Th data with the modern circulation or a state of no flow, we assume the same uncertainty for the ^{231}Pa transport equation (6) as for the analysis of water column [Pa] data ($\sqrt{C_G} = \beta_{231}$V). Likewise, the normalized adjustment or residual, $(\tilde{x} - x_o)/\sqrt{C_o}$, is used as a measure of the consistency of the data with each circulation scheme.

[56] We find that for the modern circulation, only 3% (1 of 30) of the adjustments in the Holocene [Pa] values near core locations exceed $2\sqrt{C_o}$ (in absolute magnitude) for both approaches of estimating $[Th]_p$ (Figure 7). Thus, the Holocene ^{231}Pa/^{230}Th data show a comparable degree of consistency with the modern circulation as the water column [Pa] data which have 8% (7 of 83) of its adjustments exceeding $2\sqrt{C_o}$ (section 3.4). For both approaches of estimating $[Th]_p$, the normalized adjustments in [Pa] values near core locations average to less than 0.2, indicating a small bias.

[57] In contrast, the adjustments of Holocene [Pa] values near core locations to the state of no flow are positively biased, with 23% (7 of 30) of the adjustments greater than $2\sqrt{C_o}$ and an average normalized adjustment of 1.4 or 1.3, depending on whether $[Th]_p$ is taken as the average of measured values or estimated by (9) (Figure 7). The positive adjustments in [Pa] values near core locations indicate that the [Pa] values reconstructed from the sediment are generally too low to be consistent with a state of no flow.

[58] Importantly, the inversions of [Pa] estimates for the LGM lead to adjustments with a similar distribution to that of Holocene [Pa] estimates. If $[Th]_p$ is set equal to the average of water $[Th]_p$ measurements, none of the [Pa] estimates near core locations must be altered by more than $2\sqrt{C_o}$ to be compatible with the modern circulation. If $[Th]_p$ is calculated from (9), only 1 of the 30 [Pa] estimates near core locations (3%) must be altered by more than $2\sqrt{C_o}$ to comply with the modern circulation (Figure 8). As found with the water column [Pa] data and the [Pa] values reconstructed from core tops, the adjustments of [Pa] estimates for the LGM to a state of no flow are positively biased, with 12 out of 30 (40%) total adjustments greater than $2\sqrt{C_o}$.

[59] Finally, the combination of [Pa] estimates for H1 with the modern circulation requires that only 2 out of 14 (14%) of [Pa] reconstructed near core locations be modified by more than $2\sqrt{C_o}$ if $[Th]_p$ is set equal to the average of water column $[Th]_p$ data (Figure 9). This number decreases to 1 (7%) if $[Th]_p$ is obtained from (9). Importantly, a state of no flow is less consistent with the [Pa] estimates, with 5 or 8 adjustments out of 14 (35% or 57%) exceeding $2\sqrt{C_o}$, depending on the method of estimating $[Th]_p$.

5. Discussion

5.1. Water Column ^{231}Pa Data

[60] Measurements of [Pa] in the water column in the Atlantic Ocean can be brought into consistency with the modern circulation if plausible assumptions are made about (1) the large-scale distribution of the tracer and (2) the uncertainties in our current understanding of the transport of ^{231}Pa in the deep sea. The [Pa] measurements from the Angola and Cape basins in the eastern South Atlantic [*Scholten et al.* [2008] are the least consistent with our estimate of the modern circulation. The values of total ^{231}Pa activity measured in these basins are the highest in the Atlantic Ocean (Figure 4a). *Scholten et al.* [2008] invoked

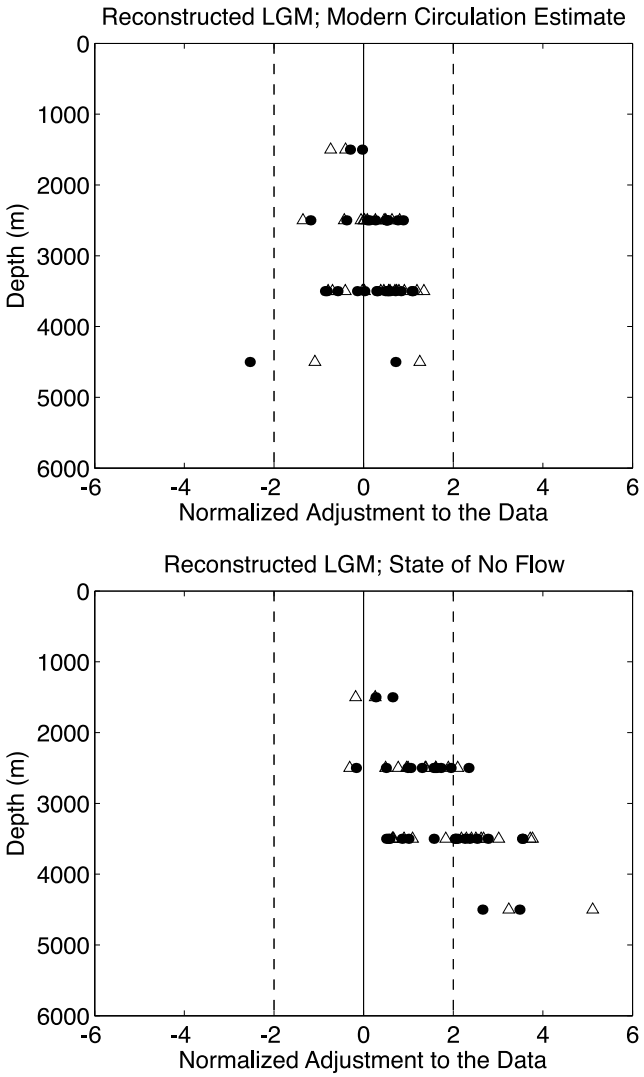

Figure 8. Same as Figure 7 but with LGM data.

the export of ^{231}Pa to the South Atlantic from the north to explain the factor of two difference between their [Pa] data and [Pa] data for the Labrador Sea [*Moran et al.*, 2002]. On the other hand, at similar latitudes, the values of [Pa] are much lower in the western Atlantic Ocean than in the eastern Atlantic Ocean (Figure 4a). Observational evidence has been reported for (1) southward transport of NADW along the western boundary in the Brazil Basin [e.g., *De Madron and Weatherly*, 1994; *Hogg and Owens*, 1999; *Weatherly et al.*, 2000] and (2) a northward transport into the Cape Basin of Antarctic Bottom Water [*Stramma and England*, 1999] and Upper Circumpolar Deep Water [*Arhan et al.*, 2003]. Additional measurements of [Pa] in these different water masses may improve understanding of the pronounced zonal difference in [Pa] in the South Atlantic.

5.2. Sediment $^{231}Pa/^{230}Th$ Data

[61] The sediment $^{231}Pa/^{230}Th$ data for the Holocene, LGM, and H1 can also be brought into consistency with the modern circulation if plausible assumptions are made about the uncertainties involved in the analysis of these data. For each time interval, the adjustments of [Pa] estimates near core locations show similar distributions, diminishing the need for different circulations to explain these data. For each interval the adjustments to a state of no flow are generally more positive than the adjustments to the modern circulation, indicating the [Pa] values implied by the sediment $^{231}Pa/^{230}Th$ data are too low to be explained purely by particle scavenging. Thus, each sediment data set (Holocene, LGM, and H1) appears to be more compatible with the modern circulation than with a state of no circulation.

[62] These results are consistent with previous studies which concluded that sediment $^{231}Pa/^{230}Th$ measurements in LGM sediments from the Atlantic Ocean do not require a circulation different from today [*Yu et al.*, 1996; *Marchal et al.*, 2000]. These studies are expanded here in three significant ways. First, our results are based on a three-dimensional model of the modern circulation which is shown to be consistent, in the least squares sense, with both hydrographic observations and water column ^{231}Pa mea-

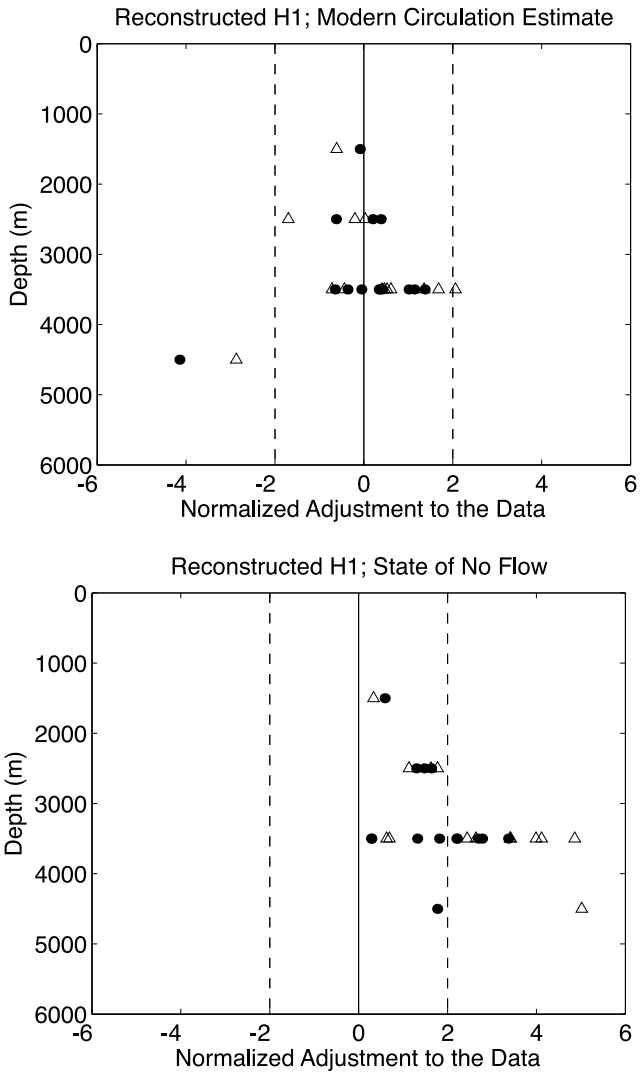

Figure 9. Same as Figure 7 but with H1 data.

surements. Second, they are based on an extended set of $^{231}Pa/^{230}Th$ data from sediment cores with improved chronologies [*McManus et al.*, 2004; *Gherardi et al.*, 2005; *Hall et al.*, 2006; *Bradtmiller et al.*, 2007; *Gherardi et al.*, 2009; Bradtmiller, unpublished data, 2009]. Finally, our analysis relies on an inverse method that formally considers the uncertainties both in the distribution of the water property ([Pa]) reconstructed from the sediment and in our understanding of the transport of this property in the ocean. Thus, the conclusion that $^{231}Pa/^{230}Th$ data for Atlantic LGM sediments do not require a circulation different from the modern is likely given a more rigorous basis.

[63] Additionally, our analysis has been extended to include sediment $^{231}Pa/^{230}Th$ measurements from the Atlantic Ocean during H1 (Figure 9). Our results show that, while [Pa] reconstructed from $^{231}Pa/^{230}Th$ measurements in Bermuda Rise sediments (core OCE326-GGC5) appears too high to be consistent with the modern circulation as previously claimed [*McManus et al.*, 2004], the majority of sediment $^{231}Pa/^{230}Th$ data for H1 actually appear consistent with the modern circulation. It is likely that $^{231}Pa/^{230}Th$ data for core OCE326-GGC5 could also be brought into consistency with the modern circulation, should a relatively high value of k_{Pa} be assumed near the core location (a higher k_{Pa} would imply a lower [Pa] in the bottom water and hence a better consistency with the modern circulation). Whereas evidence exists for high abundance of diatom frustules in Bermuda Rise sediments during H1 [*Gil et al.*, 2009; *Lippold et al.*, 2009], its implication for the partition K_d, and hence k_{Pa}, remains unclear. Nevertheless, our results underscore (1) the potential pitfall in making inferences from $^{231}Pa/^{230}Th$ data at a single site, and (2) the importance of an extensive set of data for providing useful constraints on paleocirculations [e.g., *Luo et al.*, 2010].

[64] Our result that Atlantic sediment $^{231}Pa/^{230}Th$ data for the LGM and H1 do not require a circulation different from the modern is in apparent contradiction with conclusions reached in recent studies. *Gherardi et al.* [2009] concluded that elements of the circulation in the North Atlantic Ocean were different during LGM and H1 by visually comparing vertical profiles of $^{231}Pa/^{230}Th$ established from measurements on cores originating from very different longitudes (from 9°36′W to 57°35′W) and latitudes (from 33°42′N to 58°58′N). Additionally, as this paper was in revision, *Negre et al.* [2010] published a new sediment $^{231}Pa/^{230}Th$ record from the Cape Basin (17°20′E, 34°43′S, water depth 2440 m). This $^{231}Pa/^{230}Th$ record (not included in our above analysis) was compared with $^{231}Pa/^{230}Th$ data from North Atlantic cores to argue for the dominance of a northward flow from the Southern Ocean during the LGM, that is, a reversed situation compared to the dominance of the southward flow of NADW from the North Atlantic today. We have checked that the addition of this record in our analysis does not change our above results (the fractions of [Pa] adjustments larger than $2\sqrt{C_o}$ which are reported above are modified by less than 1% for each time interval: Holocene, LGM, and H1) (see Figure S6 in the auxiliary material). Our work does not imply that the conclusions in these studies are not accurate. Rather it implies that they are sensitive to uncertainties in the spatial distribution of ^{231}Pa during these time intervals, as well as to uncertainties in our understanding of ^{231}Pa transport in the ocean (e.g., effects of particle scavenging).

5.3. Limitations of ^{231}Pa Model

[65] A major limitation and source of uncertainty in our ^{231}Pa model is that the effects of eddy mixing are not represented explicitly. This approach [see also *LeGrand and Wunsch*, 1995; *Huybers et al.*, 2007; *Marchal and Curry*, 2008] is largely motivated by simplicity. Microstructure observations suggest that diapycnal diffusivity can vary by orders of magnitude in the abyssal Atlantic with highest values near rough topography [*Polzin et al.*, 1997; *St. Laurent et al.*, 2001; *Kunze et al.*, 2006]. Likewise, results from float trajectories and eddy resolving models indicate that lateral or isopycnal transport by oceanic eddies is very complex: the lateral diffusivity can exhibit very large horizontal variations [e.g., *Figueroa*, 1994; *Berloff et al.*, 2002; *Kamenkovich et al.*, 2009], lateral diffusion can be anisotropic with a dominant zonal component [e.g., *Figueroa and Olson*, 1994; *Ollitrault and Colin de Verdière*, 2002], and the direction of eddy tracer flux can be downgradient in some regions and upgradient in others [e.g., *Lee et al.*, 1997; *Wilson and Williams*, 2006]. *Ladd and Thompson* [1998] concluded from results with an eddy-resolving model that in order to realistically reproduce the effects of eddies on tracer transport in an abyssal basin, one of two ingredients is needed: either a realistic mean flow field (including the eddy-driven mean flow) or an anisotropic eddy diffusivity that in some sense reflects the eddy-driven mean flow field. In spite of this complexity, future studies based on inverse methods could build upon this work by exploring the role of eddy mixing in the interpretation of sediment $^{231}Pa/^{230}Th$ data.

[66] The model is further limited by uncertainties in the scavenging of ^{231}Pa in the ocean. Although an effort is made to incorporate present knowledge about particle distribution and k_{Pa} in the Atlantic Ocean, it is likely that our description of the removal of Pa from the water column remains approximate. For example, a simple representation of the distribution of k_{Pa} is used, whereby a distinct but uniform value of k_{Pa} is assumed in three abyssal regions (along the western boundary, and north and south of 40°S) based on data from a few locations. Given the sparse coverage of these data, this approach appears appropriate, however it should be refined as more data become available. Observational estimates of the partitioning between dissolved and particulate forms, as well as of the concentration of suspended particles, are critically needed to better understand the removal of ^{231}Pa to the sediment. Such estimates should lead to more detailed descriptions of particle scavenging for use in large-scale models [e.g., *Siddall et al.*, 2005; *Dutay et al.*, 2009] and better estimates of model uncertainties. Particularly valuable would be paired measurements of dissolved and particulate ^{231}Pa activity in bottom nepheloid layers.

6. Conclusions and Perspectives

[67] Atlantic sediment $^{231}Pa/^{230}Th$ data for the Holocene, LGM, and H1 all appear to be generally consistent with the

modern circulation given the uncertainties involved in the analysis of these data. This result resonates with the findings of earlier studies which showed, based on other types of sediment data ($\delta^{13}C$ and $\delta^{18}O$ in benthic foraminifera), that the bulk of the data for the Atlantic during the LGM appears compatible with the modern circulation if due regard is given to data and/or model errors [*LeGrand and Wunsch*, 1995; *Gebbie and Huybers*, 2006; *Marchal and Curry*, 2008]. It must be emphasized that we do *not* conclude that the $^{231}Pa/^{230}Th$ data sets imply the H1 and LGM circulations to be the same as modern. Rather, we conclude that given the significant uncertainties in (1) the spatial distribution of ^{231}Pa activity in the Atlantic Ocean during H1 and the LGM and (2) our understanding of ^{231}Pa transport in the deep sea, the $^{231}Pa/^{230}Th$ data sets from these two time intervals do not *require* different circulations from the modern. It is also shown here that the sediment $^{231}Pa/^{230}Th$ data for the Holocene, LGM, and H1 all appear less consistent with a state of no flow than they are with the modern circulation.

[68] Thus, earlier claims from sediment $^{231}Pa/^{230}Th$ data that elements of the circulation in the Atlantic Ocean during H1 or LGM have been different from the modern [*McManus et al.*, 2004; *Gherardi et al.*, 2009; *Negre et al.*, 2010] are not as robust as originally thought. Although our results do not imply that these claims are inaccurate, they do indicate that, presently, such conclusions cannot be given a rigorous foundation given the uncertainties involved in the analysis of sedimentary $^{231}Pa/^{230}Th$ data (i.e., in both the distribution and modeling of ^{231}Pa).

[69] Perhaps the greatest merit of our study is that the assumptions needed to interpret sediment $^{231}Pa/^{230}Th$ data in terms of circulation are clarified. Hence our study allows one to identify and legitimate several perspectives. First, significant uncertainties remain in the estimation of the modern, climatologic circulation at abyssal depths due, for example, to uncertainties in the density distribution and in the geostrophic approximation. This state of affairs is detrimental to the interpretation of sediment records because the reference state, the modern circulation, to which these data should be compared is not completely understood. Thus, more hydrographic observations, including direct measurements of velocity [e.g., *Hogg and Owens*, 1999], are needed to better constrain the time-mean circulation in the subthermocline region. Second, more measurements of ^{231}Pa and ^{230}Th in the water column, such as those provided by the ongoing program GEOTRACES (http://www.geotraces.org), are required to further our understanding of the distribution and behavior of these nuclides and to enhance the effectiveness of their use in chemical oceanography and paleoceanography. A more extensive database of seawater ^{230}Th measurements would also help constrain the modern abyssal circulation [e.g., *Marchal et al.*, 2007]. Finally, increased spatial coverage of $^{231}Pa/^{230}Th$ data for well-dated sediment cores is also required to help determine possible differences in circulation for different time intervals of the recent geologic past.

[70] **Acknowledgments.** We would like to thank Mark Siddall, Carl Wunsch, Jake Gebbie, and three anonymous reviewers for helpful comments on an earlier version of this manuscript. Jeanne Gherardi and Ian Hall kindly made their sediment core data available to us. O.M. acknowledges the support from the U.S. National Science Foundation. J.F.M. acknowledges support from the U.S. National Science Foundation and the Comer Research and Education Foundation.

References

Anderson, R. F., M. P. Bacon, and P. G. Brewer (1983), Removal of ^{230}Th and ^{231}Pa from the open ocean, *Earth Planet. Sci. Lett.*, *62*(1), 7–23, doi:10.1016/0012-821X(83)90067-5.

Arhan, M., H. Mercier, and Y.-H. Park (2003), On the deep water circulation of the eastern south Atlantic Ocean, *Deep Sea Res., Part I*, *50*, 889–916, doi:10.1016/S0967-0637(03)00072-4.

Bacon, M. P., and R. F. Anderson (1982), Distribution of thorium isotopes between dissolved and particulate forms in the deep sea, *J. Geophys. Res.*, *87*, 2045–2056, doi:10.1029/JC087iC03p02045.

Baringer, M. O., and J. F. Price (1997), Mixing and spreading of the Mediterranean outflow, *J. Phys. Oceanogr.*, *27*(8), 1654–1677, doi:10.1175/1520-0485(1997)027<1654:MASOTM>2.0.CO;2.

Berloff, P. S., J. C. McWilliams, and A. Bracco (2002), Material transport in oceanic gyres. Part I: Phenomenology, *J. Phys. Oceanogr.*, *32*(3), 764–796, doi:10.1175/1520-0485(2002)032<0764:MTIOGP>2.0.CO;2.

Biscaye, P. E., and S. L. Eittreim (1977), Suspended particulate loads and transports in nepheloid layer of abyssal Atlantic Ocean, *Mar. Geol.*, *23*(1–2), 155–172, doi:10.1016/0025-3227(77)90087-1.

Bishop, J. K. B. (1999), Transmissometer measurement of POC, *Deep Sea Res., Part I*, *46*, 353–369, doi:10.1016/S0967-0637(98)00069-7.

Bradtmiller, L. I., R. F. Anderson, M. Q. Fleisher, and L. H. Burckle (2007), Opal burial in the equatorial Atlantic Ocean over the last 30 ka: Implications for glacial-interglacial changes in the ocean silicon cycle, *Paleoceanography*, *22*, PA4216, doi:10.1029/2007PA001443.

Bretherton, F. P., R. E. Davis, and C. B. Fandry (1976), Technique for objective analysis and design of oceanographic experiments applied to MODE-73, *Deep Sea Res. Oceanogr. Abstr.*, *23*, 559–582.

Brewer, P. G., D. W. Spencer, P. E. Biscaye, A. Hanley, P. L. Sachs, C. L. Smith, S. Kadar, and J. Fredericks (1976), Distribution of particulate matter in Atlantic Ocean, *Earth Planet. Sci. Lett.*, *32*(2), 393–402, doi:10.1016/0012-821X(76)90080-7.

Broecker, W. S. (1979), A revised estimate for the radiocarbon age of North Atlantic deep water, *J. Geophys. Res.*, *84*, 3218–3226, doi:10.1029/JC084iC06p03218.

Bryden, H. L., H. R. Longworth, and S. A. Cunningham (2005), Slowing of the Atlantic meridional overturning circulation at 25°N, *Nature*, *438*, 655–657, doi:10.1038/nature04385.

Chase, Z., R. F. Anderson, M. Q. Fleisher, and P. W. Kubik (2002), The influence of particle composition and particle flux on scavenging of Th, Pa and Be in the ocean, *Earth Planet. Sci. Lett.*, *204*(1–2), 215–229, doi:10.1016/S0012-821X(02)00984-6.

Cheng, H., R. L. Edwards, J. Hoff, C. D. Gallup, D. A. Richards, and Y. Asmerom (2000), The half-lives of uranium-234 and thorium-230, *Chem. Geol.*, *169*(1–2), 17–33, doi:10.1016/S0009-2541(99)00157-6.

De Madron, X. D., and G. Weatherly (1994), Circulation, transport and bottom boundary layers of the deep currents in the Brazil Basin, *J. Mar. Res.*, *52*(4), 583–638, doi:10.1357/0022240943076975.

Dutay, J.-C., F. Lacan, M. Roy-Barman, and L. Bopp (2009), Influence of particle size and type on ^{231}Pa and ^{230}Th simulation with a global coupled biogeochemical-ocean general circulation model: A first approach, *Geochem. Geophys. Geosyst.*, *10*, Q01011, doi:10.1029/2008GC002291.

Fasullo, J. T., and K. E. Trenberth (2008), The annual cycle of the energy budget. Part II: Meridional structures and poleward transports, *J. Clim.*, *21*(10), 2313–2325, doi:10.1175/2007JCLI1936.1.

Figueroa, H. A. (1994), Eddy resolution versus eddy diffusion in a double gyre GCM. Part II: Mixing of passive tracers, *J. Phys. Oceanogr.*, *24*(2), 387–402, doi:10.1175/1520-0485(1994)024<0387:ERVEDI>2.0.CO;2.

Figueroa, H. A., and D. B. Olson (1994), Eddy resolution versus eddy diffusion in a double gyre GCM. Part I: The Lagrangian and Eulerian description, *J. Phys. Oceanogr.*, *24*(2), 371–386, doi:10.1175/1520-0485(1994)024<0371:ERVEDI>2.0.CO;2.

François, R., M. Frank, M. M. Rutgers van der Loeff, and M. P. Bacon (2004), ^{230}Th normalization: An essential tool for interpreting sedimentary fluxes during the late Quaternary, *Paleoceanography*, *19*, PA1018, doi:10.1029/2003PA000939.

Gebbie, G., and P. Huybers (2006), Meridional circulation during the Last Glacial Maximum explored through a combination of South Atlantic $\delta^{18}O$ observations and a geostrophic inverse model, *Geochem. Geophys. Geosyst.*, *7*, Q11N07, doi:10.1029/2006GC001383.

Gherardi, J. M., L. Labeyrie, J. F. McManus, R. Francois, L. C. Skinner, and E. Cortijo (2005), Evidence from the northeastern Atlantic basin for variability in the rate of the meridional overturning circulation through the last deglaciation, *Earth Planet. Sci. Lett.*, *240*(3–4), 710–723, doi:10.1016/j.epsl.2005.09.061.

Gherardi, J.-M., L. Labeyrie, S. Nave, R. Francois, J. F. McManus, and E. Cortijo (2009), Glacial-interglacial circulation changes inferred from $^{231}Pa/^{230}Th$ sedimentary record in the North Atlantic region, *Paleoceanography*, *24*, PA2204, doi:10.1029/2008PA001696.

Gherardi, J.-M., Y. Luo, R. Francois, J. F. McManus, S. E. Allen, and L. Labeyrie (2010), Reply to comment by S. Peacock on "Glacial-interglacial circulation changes inferred from $^{231}Pa/^{230}Th$ sedimentary record in the North Atlantic region", *Paleoceanography*, *25*, PA2207, doi:10.1029/2009PA001867.

Gil, I. M., L. D. Keigwin, and F. G. Abrantes (2009), Deglacial diatom productivity and surface ocean properties over the Bermuda Rise, northeast Sargasso Sea, *Paleoceanography*, *24*, PA4101, doi:10.1029/2008PA001729.

Gourestki, V. V., and K. P. Koltermann (2004), WOCE global hydrographic climatology, *Tech. Rep. 35*, 54 pp., Bundesamtes für Seeschifffahrt und Hydrogr., Hamburg, Germany.

Guihou, A., S. Pichat, S. Nave, A. Govin, L. Labeyrie, E. Michel, and C. Waelbroeck (2010), Late slowdown of the Atlantic Meridional Overturning Circulation during the Last Glacial Inception: New constraints from sedimentary ($^{231}Pa/^{230}Th$), *Earth Planet. Sci. Lett.*, *289*(3–4), 520–529, doi:10.1016/j.epsl.2009.11.045.

Hall, I. R., S. B. Moran, R. Zahn, P. C. Knutz, C.-C. Shen, and R. L. Edwards (2006), Accelerated drawdown of meridional overturning in the late-glacial Atlantic triggered by transient pre-H event freshwater perturbation, *Geophys. Res. Lett.*, *33*, L16616, doi:10.1029/2006GL026239.

Heinrich, H. (1988), Origin and consequences of cyclic ice rafting in the northeast Atlantic-Ocean during the past 130,000 years, *Quat. Res.*, *29*(2), 142–152, doi:10.1016/0033-5894(88)90057-9.

Hemming, S. R. (2004), Heinrich events: Massive late Pleistocene detritus layers of the North Atlantic and their global climate imprint, *Rev. Geophys.*, *42*, RG1005, doi:10.1029/2003RG000128.

Henderson, G. M., and R. F. Anderson (2003), The U-series toolbox for paleoceanography, *Rev. Mineral. Geochem.*, *52*, 493–531, doi:10.2113/0520493.

Hogg, N. G., and W. B. Owens (1999), Direct measurement of the deep circulation within the Brazil Basin, *Deep Sea Res., Part II*, *46*, 335–353, doi:10.1016/S0967-0645(98)00097-6.

Hogg, N. G., G. Siedler, and W. Zenk (1999), Circulation and variability at the southern boundary of the Brazil Basin, *J. Phys. Oceanogr.*, *29*(2), 145–157, doi:10.1175/1520-0485(1999)029<0145:CAVATS>2.0.CO;2.

Huybers, P., G. Gebbie, and O. Marchal (2007), Can paleoceanographic tracers constrain meridional circulation rates?, *J. Phys. Oceanogr.*, *37*(2), 394–407, doi:10.1175/JPO3018.1.

Kamenkovich, I., P. Berloff, and J. Pedlosky (2009), Anisotropic material transport by eddies and eddy-driven currents in a model of the North Atlantic, *J. Phys. Oceanogr.*, *39*(12), 3162–3175, doi:10.1175/2009JPO4239.1.

Keigwin, L. D., and E. A. Boyle (2008), Did North Atlantic overturning halt 17,000 years ago?, *Paleoceanography*, *23*, PA1101, doi:10.1029/2007PA001500.

Kendall, M. G., and J. D. Gibbons (1990), *Rank Correlation Methods*, 5th ed., 260 pp., Oxford Univ. Press, New York.

Krishnaswami, S., D. Lal, B. L. K. Somayajulu, R. F. Weiss, and H. Craig (1976), Large-volume in situ filtration of deep pacific waters: Mineralogical and radioisotope studies, *Earth Planet. Sci. Lett.*, *32*(2), 420–429, doi:10.1016/0012-821X(76)90082-0.

Krishnaswami, S., M. M. Sarin, and B. L. K. Somayajulu (1981), Chemical and radiochemical investigations of surface and deep particles of the Indian Ocean, *Earth Planet. Sci. Lett.*, *54*(1), 81–96, doi:10.1016/0012-821X(81)90071-6.

Kunze, E., E. Firing, J. M. Hummon, T. K. Chereskin, and A. M. Thurnherr (2006), Global abyssal mixing inferred from lowered ADCP shear and CTD strain profiles, *J. Phys. Oceanogr.*, *36*(8), 1553–1576, doi:10.1175/JPO2926.1.

Ladd, C., and L. Thompson (1998), The influence of eddies on tracer transport in the abyssal ocean, *J. Phys. Oceanogr.*, *28*(9), 1717–1738, doi:10.1175/1520-0485(1998)028<1717:TIOEOT>2.0.CO;2.

Lee, M. M., D. P. Marshall, and R. G. Williams (1997), On the eddy transfer of tracers: Advective or diffusive?, *J. Mar. Res.*, *55*(3), 483–505, doi:10.1357/0022240973224346.

LeGrand, P., and C. Wunsch (1995), Constraints from paleotracer data on the North Atlantic circulation during the Last Glacial Maximum, *Paleoceanography*, *10*, 1011–1045, doi:10.1029/95PA01455.

Lippold, J., J. Grützner, D. Winter, Y. Lahaye, A. Mangini, and M. Christl (2009), Does sedimentary $^{231}Pa/^{230}Th$ from the Bermuda Rise monitor past Atlantic Meridional Overturning Circulation?, *Geophys. Res. Lett.*, *36*, L12601, doi:10.1029/2009GL038068.

Luo, Y., R. Francois, and S. E. Allen (2010), Sediment $^{231}Pa/^{230}Th$ as a recorder of the rate of the Atlantic meridional overturning circulation: Insights from a 2-D model, *Ocean Sci.*, *6*, 381–400, doi:10.5194/os-6-381-2010.

Marchal, O., and W. B. Curry (2008), On the abyssal circulation in the glacial Atlantic, *J. Phys. Oceanogr.*, *38*(9), 2014–2037, doi:10.1175/2008JPO3895.1.

Marchal, O., R. Francois, T. F. Stocker, and F. Joos (2000), Ocean thermohaline circulation and sedimentary $^{231}Pa/^{230}Th$ ratio, *Paleoceanography*, *15*, 625–641, doi:10.1029/2000PA000496.

Marchal, O., R. Francois, and J. Scholten (2007), Contribution of ^{230}Th measurements to the estimation of the abyssal circulation, *Deep Sea Res., Part I*, *54*, 557–585, doi:10.1016/j.dsr.2007.01.002.

Martel, F., and C. Wunsch (1993), The North Atlantic Circulation in the early 1980s—An estimate from inversion of a finite-difference model, *J. Phys. Oceanogr.*, *23*(5), 898–924, doi:10.1175/1520-0485(1993)023<0898:TNACIT>2.0.CO;2.

McManus, J. F., R. Francois, J. M. Gherardi, L. D. Keigwin, and S. Brown-Leger (2004), Collapse and rapid resumption of Atlantic meridional circulation linked to deglacial climate changes, *Nature*, *428*, 834–837, doi:10.1038/nature02494.

Moran, S. B., C.-C. Shen, S. E. Weinstein, L. H. Hettinger, J. H. Hoff, H. N. Edmonds, and R. L. Edwards (2001), Constraints on deep water age and particle flux in the equatorial and South Atlantic Ocean based on seawater ^{231}Pa and ^{230}Th data, *Geophys. Res. Lett.*, *28*, 3437–3440, doi:10.1029/2001GL013339.

Moran, S. B., C. C. Shen, H. N. Edmonds, S. E. Weinstein, J. N. Smith, and R. L. Edwards (2002), Dissolved and particulate ^{231}Pa and ^{230}Th in the Atlantic Ocean: Constraints on intermediate/deep water age, boundary scavenging, and $^{231}Pa/^{230}Th$ fractionation, *Earth Planet. Sci. Lett.*, *203*(3–4), 999–1014, doi:10.1016/S0012-821X(02)00928-7.

Morris, M. Y., M. M. Hall, L. C. St. Laurent, and N. G. Hogg (2001), Abyssal mixing in the Brazil Basin, *J. Phys. Oceanogr.*, *31*(11), 3331–3348, doi:10.1175/1520-0485(2001)031<3331:AMITBB>2.0.CO;2.

Negre, C., R. Zahn, A. L. Thomas, P. Masque, G. M. Henderson, G. Martinez-Mendez, I. R. Hall, and J. L. Mas (2010), Reversed flow of Atlantic deep water during the Last Glacial Maximum, *Nature*, *468*, 84–88, doi:10.1038/nature09508.

Nelson, D. M., P. Treguer, M. A. Brzezinski, A. Leynaert, and B. Queguiner (1995), Production and dissolution of biogenic silica in the ocean: Revised global estimates, comparison with regional data and relationship to biogenic sedimentation, *Global Biogeochem. Cycles*, *9*, 359–372, doi:10.1029/95GB01070.

Nozaki, Y., Y. Horibe, and H. Tsubota (1981), The water column distributions of thorium isotopes in the western North Pacific, *Earth Planet. Sci. Lett.*, *54*(2), 203–216, doi:10.1016/0012-821X(81)90004-2.

Ochoa, J., and N. A. Bray (1991), Water mass exchange in the Gulf of Cadiz, *Deep Sea Res., Part A*, *38*, S465–S503.

Ollitrault, M., and A. Colin de Verdière (2002), SOFAR floats reveal midlatitude intermediate North Atlantic general circulation. Part I: A Lagrangian descriptive view, *J. Phys. Oceanogr.*, *32*(7), 2020–2033, doi:10.1175/1520-0485(2002)032<2020:SFRMIN>2.0.CO;2.

Peacock, S. (2010), Comment on "Glacial-interglacial circulation changes inferred from $^{231}Pa/^{230}Th$ sedimentary record in the North Atlantic region" by J.-M. Gherardi et al., *Paleoceanography*, *25*, PA2206, doi:10.1029/2009PA001835.

Polzin, K. L., J. M. Toole, J. R. Ledwell, and R. W. Schmitt (1997), Spatial variability of turbulent mixing in the abyssal ocean, *Science*, *276*(5309), 93–96, doi:10.1126/science.276.5309.93.

Roemmich, D., and C. Wunsch (1985), Two transatlantic sections: Meridional circulation and heat flux in the subtropical North Atlantic Ocean, *Deep Sea Res., Part A*, *32*, 619–664, doi:10.1016/0198-0149(85)90070-6.

Rutgers van der Loeff, M. M., and G. W. Berger (1993), Scavenging of ^{230}Th and ^{231}Pa near the antarctic polar front in the South-Atlantic, *Deep Sea Res., Part I*, *40*, 339–357, doi:10.1016/0967-0637(93)90007-P.

Schmitz, W. J., Jr., and M. S. McCartney (1993), On the North Atlantic Circulation, *Rev. Geophys.*, *31*, 29–49, doi:10.1029/92RG02583.

Scholten, J. C., M. M. Rutgers van der Loeff, and A. Michel (1995), Distribution of ^{230}Th and ^{231}Pa in the water column in relation to the ventilation of the deep Arctic basins, *Deep Sea Res., Part II*, *42*, 1519–1531, doi:10.1016/0967-0645(95)00052-6.

Scholten, J. C., J. Fietzke, A. Mangini, C. D. Garbe-Schbnberg, A. Eisenhauer, R. Schneider, and P. Stoffers (2008), Advection and scavenging: Effects on ^{230}Th and ^{231}Pa distribution off Southwest Africa, *Earth Planet. Sci. Lett.*, *271* (1–4), 159–169, doi:10.1016/j.epsl.2008.03.060.

Siddall, M., G. M. Henderson, N. R. Edwards, M. Frank, S. A. Muller, T. F. Stocker, and F. Joos (2005), 231Pa-231/Th-210 fractionation by ocean transport, biogenic particle flux and particle type, *Earth Planet. Sci. Lett.*, *237*(1–2), 135–155, doi:10.1016/j.epsl.2005.05.031.

Siddall, M., T. F. Stocker, G. M. Henderson, F. Joos, M. Frank, N. R. Edwards, S. P. Ritz, and S. A. Muller (2007), Modeling the relationship between $^{231}Pa/^{230}Th$ distribution in North Atlantic sediment and Atlantic meridional overturning circulation, *Paleoceanography*, *22*, PA2214, doi:10.1029/2006PA001358.

St. Laurent, L. C., J. M. Toole, and R. W. Schmitt (2001), Buoyancy forcing by turbulence above rough topography in the abyssal Brazil Basin, *J. Phys. Oceanogr.*, *31*(12), 3476–3495, doi:10.1175/1520-0485(2001)031<3476:BFBTAR>2.0.CO;2.

Stramma, L., and M. England (1999), On the water masses and mean circulation of the South Atlantic Ocean, *J. Geophys. Res.*, *104*, 20,863–20,883, doi:10.1029/1999JC900139.

Talley, L. D. (2003), Shallow, intermediate, and deep overturning components of the global heat budget, *J. Phys. Oceanogr.*, *33*(3), 530–560, doi:10.1175/1520-0485(2003)033<0530:SIADOC>2.0.CO;2.

Trenberth, K. E., and J. M. Caron (2001), Estimates of meridional atmosphere and ocean heat transports, *J. Clim.*, *14*(16), 3433–3443, doi:10.1175/1520-0442(2001)014<3433:EOMAAO>2.0.CO;2.

Venchiarutti, C., C. Jeandel, and M. Roy-Barman (2008), Particle dynamics study in the wake of Kerguelen Island using thorium isotopes, *Deep Sea Res., Part I*, *55*, 1343–1363, doi:10.1016/j.dsr.2008.05.015.

Walter, H. J., M. M. Rutgers van der Loeff, and H. Hoeltzen (1997), Enhanced scavenging of ^{231}Pa relative to ^{230}Th in the south Atlantic south of the Polar front: Implications for the use of the $^{231}Pa/^{230}Th$ ratio as a paleoproductivity proxy, *Earth Planet. Sci. Lett.*, *149*(1–4), 85–100, doi:10.1016/S0012-821X(97)00068-X.

Walter, H. J., W. Geibert, M. M. Rutgers van der Loeff, G. Fischer, and U. Bathmann (2001), Shallow vs. deep-water scavenging of ^{231}Pa and ^{230}Th in radionuclide enriched waters of the Atlantic sector of the Southern Ocean, *Deep Sea Res., Part I*, *48*, 471–493, doi:10.1016/S0967-0637(00)00046-7.

Weatherly, G. L., Y. Y. Kim, and E. A. Kontar (2000), Eulerian measurements of the North Atlantic Deep Water deep western boundary current at 18°S, *J. Phys. Oceanogr.*, *30*(5), 971–986, doi:10.1175/1520-0485(2000)030<0971:EMOTNA>2.0.CO;2.

Wilson, C., and R. G. Williams (2006), When are eddy tracer fluxes directed downgradient?, *J. Phys. Oceanogr.*, *36*(2), 189–201, doi:10.1175/JPO2841.1.

Wunsch, C. (1996), *The Ocean Circulation Inverse Problem*, 442 pp., Cambridge Univ. Press, Cambridge, U. K., doi:10.1017/CBO9780511629570.

Wunsch, C. (2003), Determining paleoceanographic circulations, with emphasis on the Last Glacial Maximum, *Quat. Sci. Rev.*, *22*(2–4), 371–385, doi:10.1016/S0277-3791(02)00177-4.

Wunsch, C. (2005), The total meridional heat flux and its oceanic and atmospheric partition, *J. Clim.*, *18*(21), 4374–4380, doi:10.1175/JCLI3539.1.

Yu, E.-F. (1994), Variations in the particulate flux of ^{230}Th and ^{231}Pa and paleoceanograhpic applications of the $^{231}Pa/^{230}Th$ ratio, Ph.D. thesis, 269 pp, Mass. Inst. of Technol. and Woods Hole Oceanogr. Inst., Woods Hole, Mass.

Yu, E. F., R. Francois, and M. P. Bacon (1996), Similar rates of modern and last-glacial ocean thermohaline circulation inferred from radiochemical data, *Nature*, *379*, 689–694, doi:10.1038/379689a0.

Zenk, W., G. Siedler, B. Lenz, and N. G. Hogg (1999), Antarctic Bottom Water flow through the Hunter channel, *J. Phys. Oceanogr.*, *29*(11), 2785–2801, doi:10.1175/1520-0485(1999)029<2785:ABWFTT>2.0.CO;2.

L. I. Bradtmiller, Department of Environmental Studies, Macalester College, 1600 Grand Ave., St. Paul, MN 55105, USA.

A. Burke, MIT/WHOI Joint Program in Oceanography, Woods Hole Oceanographic Institution, MS 24 Woods Hole, MA 02543, USA. (aburke@whoi.edu)

R. François, Department of Earth and Ocean Sciences, University of British Columbia, 6270 University Blvd., Vancouver, BC V6T 1Z4, Canada.

O. Marchal, Department of Geology and Geophysics, Woods Hole Oceanographic Institution, Quissett Campus, MS 23, Woods Hole, MA 02543, USA.

J. F. McManus, Department of Earth and Environmental Science, Lamont-Doherty Earth Observatory, 239 Comer Geochemistry Bldg., Palisades, NY 10964, USA.